LA-UR-17-25931
Approved for public release; distribution is unlimited.

Title: Development of Multi-physics (Multiphase CFD + MCNP) simulation for generic solution vessel power calculation

Author(s): Kim, Seung Jun
Buechler, Cynthia Eileen

Intended for: Report

Issued: 2017-07-17

Development of Multi-physics (Multiphase CFD + MCNP) simulation for generic solution vessel power calculation

Seung Jun Kim
Nuclear Engineering and Nonproliferation Division
Nuclear System Design and Analysis (NEN-5)
Los Alamos National Laboratory
Los Alamos, NM 87544

Cynthia Buechler
Accelerator Operations and Technology Division
Mechanical Design Engineering (MDE)
Los Alamos National Laboratory
Los Alamos, NM 87544

Executive Summary

The current study aims to predict the steady state power of a generic solution vessel and to develop a corresponding heat transfer coefficient correlation for a Moly99 production facility by conducting a fully coupled multi-physics simulation. A prediction of steady state power for the current application is inherently interconnected between thermal hydraulic characteristics (i.e. Multiphase computational fluid dynamics solved by ANSYS-Fluent 17.2) and the corresponding neutronic behavior (i.e. particle transport solved by MCNP6.2) in the solution vessel. Thus, the development of a coupling methodology is vital to understand the system behavior at a variety of system design and postulated operating scenarios. In this study, we report on the k-effective (keff) calculation for the baseline solution vessel configuration with a selected solution concentration using MCNP K-code modeling. The associated correlation of thermal properties (e.g. density, viscosity, thermal conductivity, specific heat) at the selected solution concentration are developed based on existing experimental measurements in the open literature. The numerical coupling methodology between multiphase CFD and MCNP is successfully demonstrated, and the detailed coupling procedure is documented. In addition, improved coupling methods capturing realistic physics in the solution vessel thermal-neutronic dynamics are proposed and tested further (i.e. dynamic height adjustment, mull-cell approach). As a key outcome of the current study, a multi-physics coupling methodology between MCFD and MCNP is demonstrated and tested for four different operating conditions. Those different operating conditions are determined based on the neutron source strength at a fixed geometry condition. The steady state powers for the generic solution vessel at various operating conditions are reported, and a generalized correlation of the heat transfer coefficient for the current application is discussed. The assessment of multi-physics methodology and preliminary results from various coupled calculations (power prediction and heat transfer coefficient) can be further utilized for the system code validation and generic solution vessel design improvement.

Contents

Figures

Tables

1. Background and Introduction

Following the medical isotope shortage crisis in 2008, attention has been drawn to several alternative technologies to produce industrial grade of domestic Molybdenum-99 (approximately 85% of nuclear medicine diagnostic imaging procedures worldwide) with full consideration of a non-proliferation platform [1]. While a variety of supplementary technologies have been proposed for the production of Molybdenum-99, some of them are not yet commercially proven, and some are still in the early stage of development [2]. Therefore, National Nuclear Security Administration (NNSA) has accelerated the development of emerging technologies for domestic Moly-99 production by promoting collaborative research efforts between national laboratories and industry partners. Demonstration of domestic Molybdenum-99 production without the use of Highly Enriched Uranium (HEU) is considered a vital component for national security.

In this current study, we analyze the design concept of an accelerator driven solution vessel based Moly-99 production facility by demonstrating a fully coupled multi-physics modeling capability to predict the steady state system power of the solution vessel. A generic solution vessel with 12 cooling tubes is selected for the baseline design study. The thermal hydraulic condition of the solution vessel is characterized by using Multiphase computation fluid dynamic (MCFD), and the fission induced energy deposition is simultaneously evaluated by using MCNP. The goal for the current study is to demonstrate a well-represented multi-physics (MCFD+MCNP) methodology for generic solution vessel power calculation at the steady state condition. The correlation between the initial power calculation from the cold start condition and the saturated system power is developed, and more importantly, the system level heat transfer coefficient for the solution vessel at a range of operating conditions is produced, which could feed into the system level response code development as a key input. Figure 1 demonstrates a summarized technical path with potential deliverables from the current study.

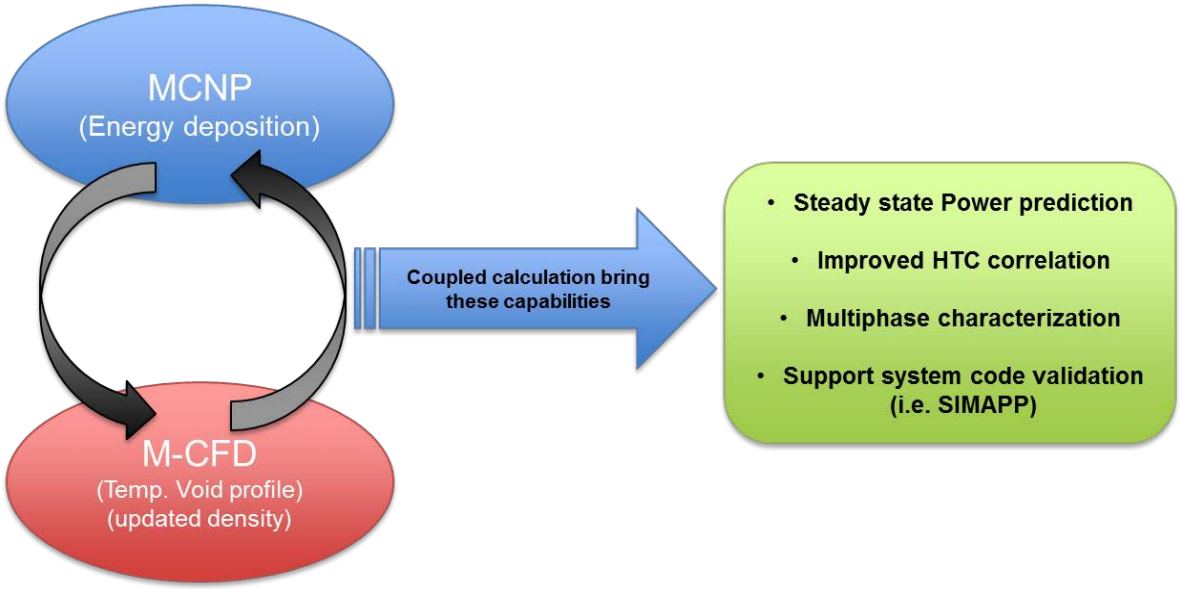

Figure 1 Schematic diagram of technical path with potential output from the coupled calculation

2. Baseline solution vessel configuration and keff calculation

2.1 Solution vessel geometry

The overarching design concept of the generic solution vessel is a subcritical system with a controlled neutron source supplied from the accelerator driven deuterium-tritium (DT) reaction. The fissile material used in the current design is a uranyl sulfate solution with a concentration

of 140g-U/L, which leads to a uranyl sulfate solution density of 1185.4 kg/m^3. The accelerator's beam energy is determined to produce a targeted neutron source with a desirable profile along the axial direction of the vacuum chamber. A moderator material is placed between vacuum chamber and the solution vessel. The cooling option in the current design includes 12 circular cooling tubes with 1.6 cm ID, an annulus shape of inner cooling channel with 0.5 cm gap, and an annulus shape of outer cooling channel with 0.5 cm gap. The combination of these cooling options is designed to promote an efficient natural circulation mechanism by extracting the heat from the solution vessel. A graphical visualization of the baseline solution vessel configuration from side and top view is reported in Figure 2. Associated dimensions of the baseline solution vessel configuration are summarized in
Table 1. Note that the dimensions of the baseline solution vessel are identically captured in both the MCFD and MCNP modeling.

Table 1 Dimensions of Baseline Solution Vessel and cooling channels

Baseline solution vessel component		Cooling channel components	
OD of vacuum	8.5 cm	Inner channel thickness	0.5 cm
OD of Moderator	16.5 cm	OD of cooling tubes	2.0 cm
Zircaloty4 wall thickness	0.5 cm	ID of cooling tubes	1.6 cm
ID of Solution vessel	17.5 cm	Outer channel thickness	0.5 cm
OD of Solution vessel	35.0 cm	Number of cooling tubes	12
Aluminum outer wall thickness	0.5 cm		
OD of pool	60 cm		

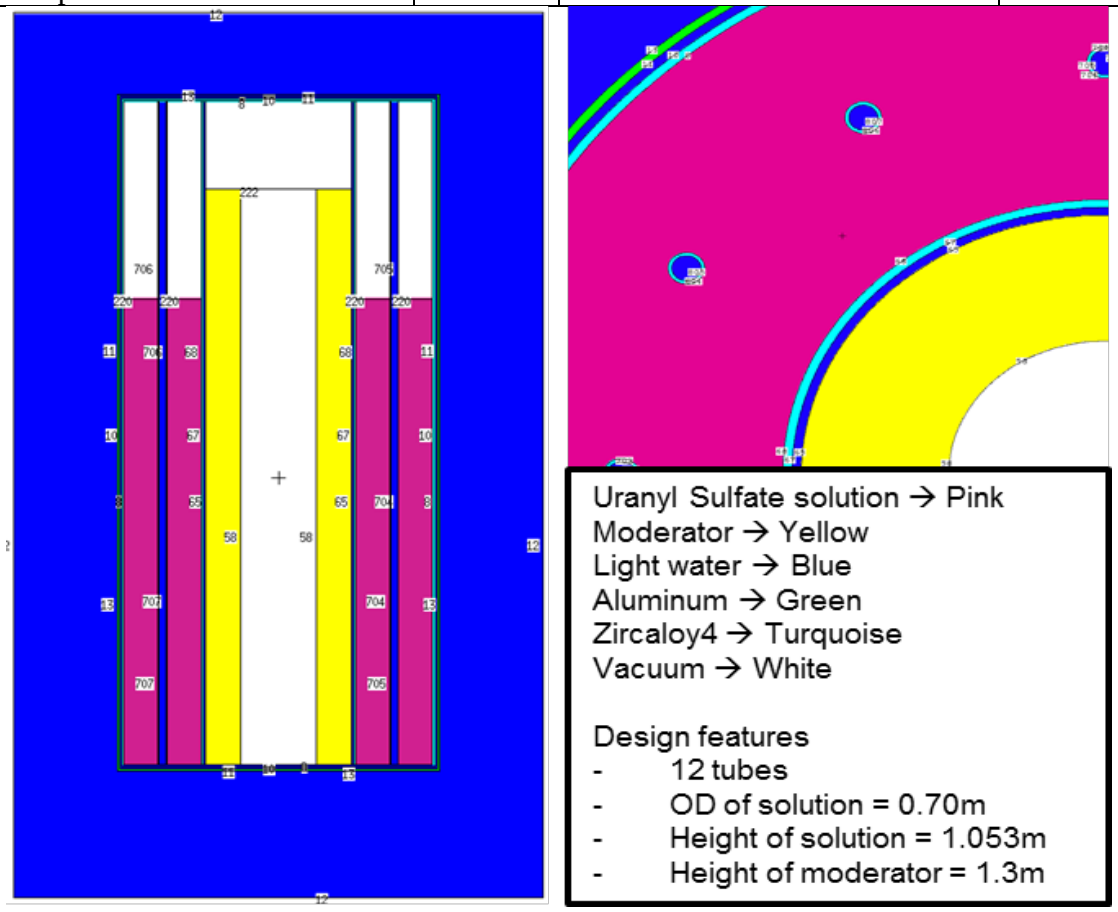

Figure 2 Schematic diagram of generic solution vessel configuration and design feature

Beam energy and normalized neutron yield profile from the DT reaction along the beamline are

calculated given the vacuum pressure of 9 Torr, and a corresponding source neutron profile calculated from MCNP is visualized in a horizontally represented system diagram (Figure 3). The beam energy linearly decreases as the beam is traveling through the vacuum chamber, and it should be noted that the beam energy is completely dissipating before the beam is approaching to the bottom of vacuum chamber. The mass stopping power method is used to calculate these beam characteristics in the vacuum chamber. In addition, the neutron production rate from the DT reaction is estimated by calculating the DT Fusion cross section. At the given vacuum pressure (i.e. 9 Torr) the maximum neutron yield from the DT reaction is observed at 60cm from the beginning of the beam traveling in the vacuum tank. As a result, the maximum power of the fission reaction is expected to take place near the middle of the solution vessel. The detailed calculation note for the beam energy and neutron yield rate along with axial direction are reported in Appendix A.

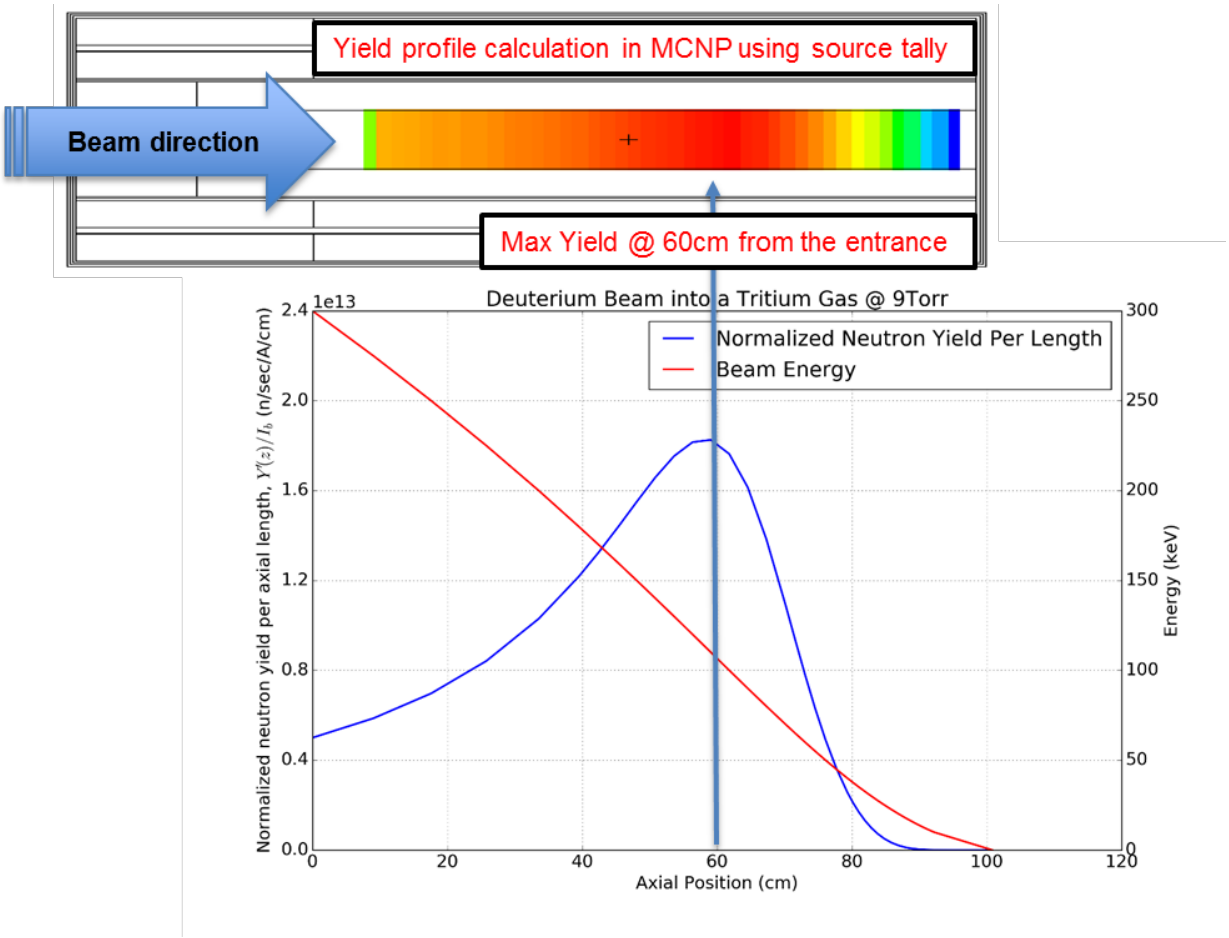

Figure 3 Normalized neutron yield per length calculation and beam energy along with axial position starting from top of solution vessel

2.2 Thermal property correlation development

To achieve high fidelity predictive capability for both the thermal hydraulic and neutron transport models, it is critical to develop reliable thermal property correlations for the solution (e.g. uranyl sulfate) at the operating condition of interest. The concentration and temperature dependent material properties for Uranyl Sulfate are summarized in Table 2. An appropriate temperature range for each property and relevant reference used for the current correlation are also indicated in the third and fourth columns. It should be noted that the correlations developed for the current application were intentionally developed for the targeted operation conditions while the experimental measurements from reference encompass a wide range of operating

conditions. Therefore, one needs to take extra care when using these correlations outside of the applicable range, which may result in an erroneous value or unphysical implication in the numerical calculation.

Table 2 Thermal properties for Uranyl Sulfate as a function of concentration and temperature

Thermal properties	**Equation (X= concentration, g-U/L, Y= temperature, C)**	**Temp. & Concentration range**	**Reference**
Density [g/mL]	$7.16e-8X^2 + 0.0013\,X - 3.43e-6\,Y^2 - 0.00019Y + 1.0068$	20-90 [C] 90-160 [g-U/L]	Mound Laboratory report [3]
Viscosity [cp]	$-6.61e-6\,X^2 + 0.0038\,X + 0.00023\,Y^2 - 0.038\,Y + 1.65$	20-90 [C] 90-160 [g-U/L]	ANL/CSE report [4]
Thermal conductivity [mW/mK]	$0.0069X^2 - 1.9X - 0.0015Y^2 + 1.19\,Y + 678.65$	20-90 [C] 90-160 [g-U/L]	ANL/CSE report [4]
Specific Heat [J/gK]	$1.64e-5X^2 - 0.0094X + 3.23e-6Y^2 - 0.00063Y + 4.34$	20-90 [C] 90-160 [g-U/L]	ANL/CSE report [4]
Surface Tension [N/m]	0.071	20-90 [C] 90-160 [g-U/L]	N/A

The development of the concentration and temperature dependent polynomial for each property was performed using the multivariable regression method in GnuPlot. The detailed calculation note is documented in Appendix B.

2.3 Keff calculation with varying solution height and concentration

To meet a desirable keff value for the startup condition in the baseline solution vessel configuration, we perform criticality calculations (i.e. Kcode calculations) with various solution heights and solution concentrations. In order to evaluate the influence of solution height on the system criticality, all other design parameters except for the solution height are fixed at the reference values given in the baseline configuration. As shown in Figure 4, the criticality of the system is gradually increasing as the solution's height elevates at a given solution concentration of 105g-U/L. This trend indicates that the increase of fissile material in the system leads to a higher keff value, as expected. More importantly, the solution concentration has to be determined to meet a desirable criticality value at the startup condition. In this study, we select the keff value of 0.98, which will provide sufficient safety margin for the subcritical system from an unexpected criticality issue. After performing the Kcode calculations, the final solution concentration was selected to be 140g-U/L as a target cold start condition, which meets the design requirement for the subcritical solution vessel. The final estimated keff is calculated to be 0.98633 with an estimated standard deviation of 0.00063. In other words, the keff value is estimated to be in the range of 0.98466 to 0.98801 with a 99 percent confidence level. Hereafter, the solution concentration of 140g-U/L is used as a reference solution condition for the current study. All of the associated solution thermal properties are calculated for this concentration using the correlations developed in the previous section.

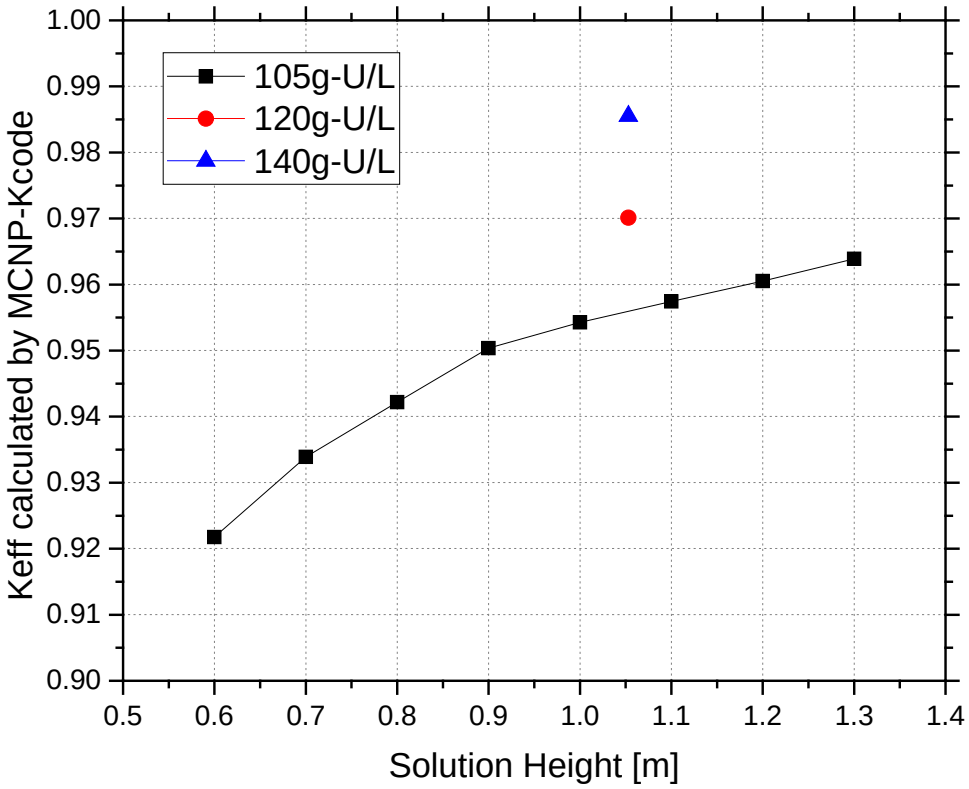

Figure 4 Keff calculation with varying solution height and concentration

3. Numerical model descriptions

3.1 MCNP model specification and energy deposition calculation

Detailed input for the MCNP model for the energy deposition calculation can be found in Appendix C. The geometry and associated material for the current application is accordingly constructed in the input file while capturing the various cooling structures (12 tube cooling, inner channel, and outer channel). Both prompt and delayed neutrons are accounted for in the energy deposition calculation. The appropriate source definition is modeled based on the normalized neutron yield profile along with the corresponding beam traveling direction. The most updated nuclear cross-section libraries, such as ENDF/B-VII, are utilized in the current simulation with full consideration of the thermal neutron scattering effect by using S(α,β) data for the light water material [5].

Two different tallies are implemented to calculate actual energy deposition in the solution vessel: 1) Fission neutron flux tally (F4MESH) and 2) heating tally (F6MESH). Both tallies are azimuthally averaged and produce a two dimensional volumetric energy profile q(r,z). In a crosscheck study between fission flux tally and heating tally, it is observed that the fission flux tally predicts a volumetric energy deposition that is higher than the heating tally in terms of energy deposition. However, this discrepancy could depend on the estimated conversion factor value (e.g. 190Mev/fission neutron) used in the flux tally. Therefore, a heating tally based energy deposition calculation method without any assumed conversion factor, is preferable to evaluate a realistic volumetric energy generation in the solution vessel. One interesting observation while using the heating tally method is that the non-fissile material (e.g. cooling tubes) is appropriately accounted for in the energy deposition calculation. This results in a little

hump effect in the location of the cooling tubes, as shown in Figure 5. Since we are only modeling the solution vessel section in the multiphase CFD calculation, the heating tally is averaged across a region containing only solution, excluding any effect of the cooling tubes in terms of energy deposition. Then the volumetric energy generation rate calculated from MCNP is fed as an input into the multiphase CFD model for the thermal hydraulic calculation in the solution vessel.

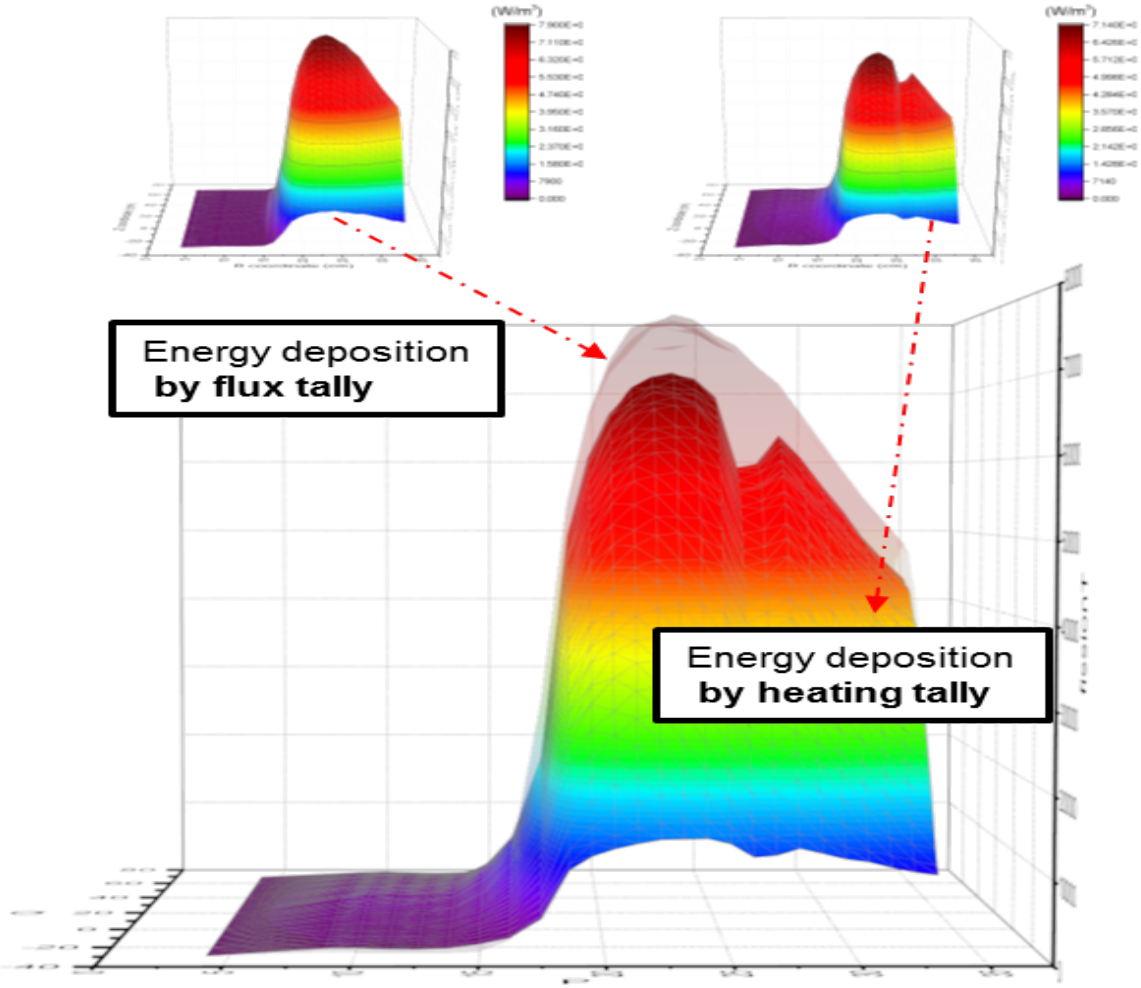

Figure 5 fission tally (F4) vs heating tally (F6) for energy deposition calculation

3.2 Multiphase CFD model specification and boundary condition

All numerical simulations described herein have been performed with ANSYS-Fluent 17.2. A three-dimensional solution vessel geometry and mesh were generated with ANSYS Design Modeler and Mesher [6]. For this particular application, the Eulerian based two-fluid model approach is selected to evaluate the characteristics of disperse bubbly flow for multiphase natural circulation application. In other words, the two fluid (liquid phase and gas phase) are resolved independently with a correlation of void fraction at each cell instead of resolving the interface of two phase. Thus, it is considered that the Eulerian based approach should be physically acceptable and economically reasonable to simulate multiphase thermal hydraulic behavior (i.e. two phase natural circulation) in the solution vessel.

Bubble generation modeled in the current Multiphase CFD practice does not involve any phase change type phenomena (i.e. no boiling or condensation). Radiolytic gas (i.e. vapor phase

bubble) is generated as a by-product of the fission reaction in the solution. Thus, the bubble generation profile is directly proportional to the power profile with a given conversion factor. A time averaged void fraction distribution and temperature distribution are calculated by solving the natural circulation characteristic in the MCFD. Note the solution density in two phases flow is a function of solution temperature and void fraction. The density and temperature profiles calculated from the MCFD model are used as key inputs for MCNP's power calculation.

3.2.1 Geometry and Mesh

Due to the axisymmetric design of the solution vessel, a 3-Dimensional 24th segmented model is constructed and meshed as shown in Figure 6. The computational domain simulated in the current study consists of a half side of cooling tube and two cooling boundaries defined by the inner and outer channels. A hexagonal dominant mesh is generated with 15 inflation layers at the cooling channel surfaces to represent the heat transfer coefficient correctly by capturing the thermal boundary layer. For the given flow regime, the non-dimensional wall distance (i.e. y+, value of the first cell at the wall) was calculated to be less than 1. This y+ evaluation indicates that the thermal boundary layer is well resolved for an accurate heat transfer coefficient calculation. The total number of mesh cells is approximately 100K, with 99.8% hexagonal cells and 0.2% wedge cells. The quality of the mesh is evaluated by monitoring the skewness, orthogonal quality, and aspect ratio, and the values for these metrics are reasonable for the current application.

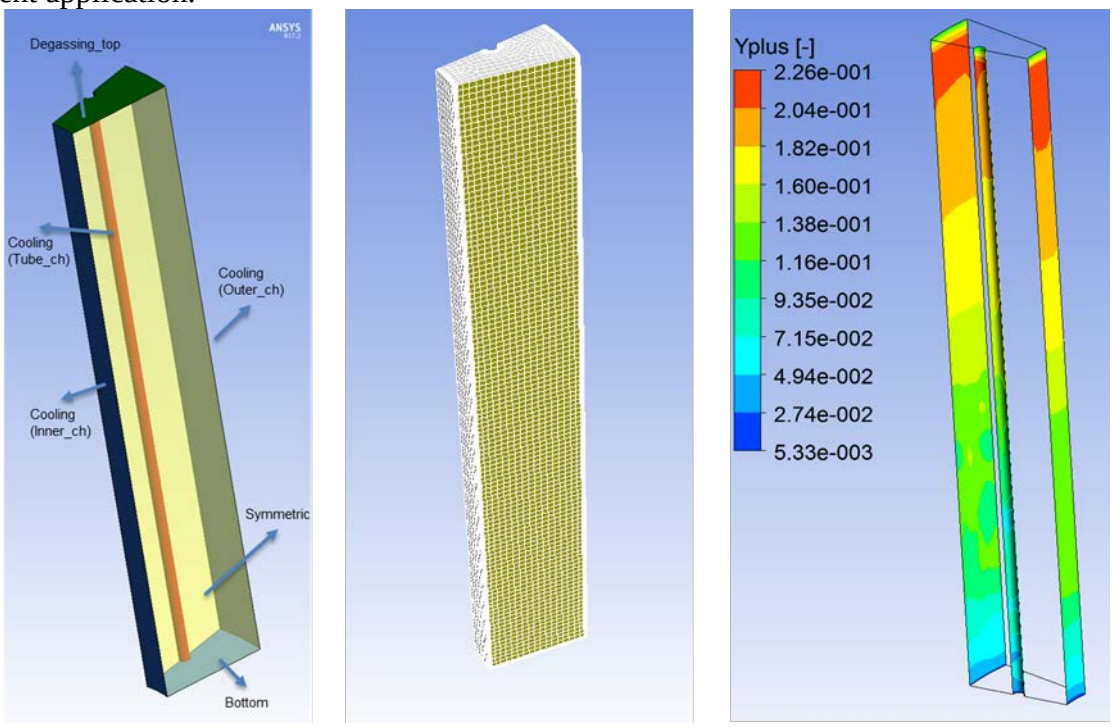

Figure 6 Boundary specification, Mesh, and Y+ value calculation at the cooling wall.

3.2.2 Boundary condition, Turbulence model, and solver setting

The multiphase CFD model selection and boundary condition specification used in the current study are summarized as below. A visual description of the boundary conditions applied can be found in Figure 6. Mathematical Navier-Stokes equations to resolve the continuity of mass, momentum, turbulence parameters, two fluid parameters (i.e. void), and energy are found in the ANSYS theory guide [6]. A set of detailed descriptions of the model used for the current application is listed below.

- Solver:
    - Space: 3-D double precision
    - Solver: pressure based
    - Temporal discretization: Steady state with Pseudo transient approach
    - Spatial Discretization
        - Green-gauss node base model for pressure gradient
        - Quick option for momentum, volume fraction, turbulence, and energy
    - Pressure-velocity coupling: Coupled method
- Viscosity Model
    - SST-kω model
    - Turbulence Dispersed Multiphase model
- Energy equation on
- Multiphase interaction model (Eulerian based two fluid approach)
    - Lift model: Tomiyama
    - Drag mode: Schiller-Naumann
    - Wall lubrication model: Antal
    - Turbulence disperse model: Simonin
    - Turbulence interaction model: Sato
    - Virtual mass: Not applied
    - Heat transfer coefficient mode: Ranz-Marshall
    - Interface area model: A symmetric model
- Boundary condition
    - Degassing boundary condition applied at the top surface of solution vessel.
    - Symmetry condition at two symmetric surfaces
    - Adiabatic wall boundary condition at the bottom of solution vessel
    - Convective heat transfer boundary condition applied at three cooling channels
        - Gnielinski correlation used for Heat Transfer Coefficient (HTC)
        - FST (Free Steam Temperature) values are calculated using the energy balance equation ($Q = \dot{m}Cp\Delta T$) for the current power level for each cooling channel.
- Material properties and power and gas generation profile
    - Polynomial material properties for both the uranyl sulfate solution and the radiolytic gas are applied.
    - Volumetric energy generation rate in the solution implemented by using a User Defined Function (UDF). The power profile is provided from the MCNP calculation.
    - Volumetric radiolytic gas generation rate in the solution also implemented by UDF.

The Shear Stress Transport k-omega turbulence model using the standard wall treatment function is selected since the turbulence in the solution it is expected to be fairly isotropic in natural circulation flow condition. Any gains in simulation fidelity with a more sophisticated turbulence model such as Reynolds Stress Model (RSM) or Large Eddy Simulation (LES) are not expected. The multiphase interaction models listed above for the current application have been evaluated by performing a thorough sensitivity study documented in a previous report [11]. In the present study, we follow the appropriate practice for multiphase models that is already investigated while admitting the maturity and applicability of the multiphase modeling is in active area of research in the MCFD field. The overall multiphase CFD model specifications are summarized in Figure 7.

Multiphase Eulerian-Eulerian (two-fluid model) based natural circulation simulation model (continuum liquid + discrete bubble)					
Type	Name	Specifications			
Mesh	Cell Number	100K (Hex type)			
Solver	Spatial & Temporal	3D (1/24th model), Pseudo transient simulation			
Turbulence Modeling	URANS	K-omega SST model			
Cell (Volumetric condition)	Power input (energy)	Power profile calculated from MCNP (UDF)			
	Bubble input (mass)	Bubble generation proportional to power (UDF)			
Material Properties Two phase(liquid + gas)	phase	Liquid (Uranyl Surface)		Radiolytic gas	
	Density	987.864+1.68197*T - 0.00343*T^2		0.8689 - 0.001281*T	
	Specific heat	3439.243 - 2.396*T + 0.0032*T^2		2303 + 0.3856*T	
	Thermal Conductivity	0.103 + 0.00204*T - 1.57e-6*T^2		0.01322 + 0.0001032*T	
	Viscosity	0.0301 - 0.000167*T + 2.37e-7*T^2		5.215e-6 + 4.737e-8*T	
	Surface Tension	~ 0.071 N/m			
Boundary condition	Cooling channels → Convective heat transfer boundary applied → Calculated based on the specific power		Inner_ch	Outer_ch	Tube_ch
		HTC	7667 W/m2-k	7661 W/m2-k	7550 W/m2-k
		T_{fst}	298.7K	294.9K	294.9K
		Thickness	0.5cm	0.5cm	0.1cm
		Material	Zircaloy4	Zircaloy4	Zircaloy4
	Degassing top	Vapor phase (gas) out only			
	Symmetric	Adiabatic			
	Bottom	Adiabatic			

*** Note: 1) HTC and FST are simultaneously updated in every iterative MCFD calculations based on the updated system power condition and related thermal hydraulic parameter. 2) The surface tension correlation used is also a function of temperature, however, the variability of surface tension in the operating temperature is negligible for the current application.

Figure 7 CFD model specifications for multiphase natural circulation application

3.3 MCNP+MCFD coupling methodology

Aforementioned numerical modeling approaches for MCNP and Multiphase-CFD (MCFD) provide high fidelity predictive capability for each physics only. For example, an MCNP simulation calculates the neutron transport and associated power profile in the solution, and MCFD predicts multiphase thermal hydraulic behavior, system level operating temperature, and void fraction for a given power profile. Due to the nature of the generic solution application, however, the thermal hydraulic behaviors (temperature and void fraction) are interconnected with the power profile calculated from neutron transport phenomenon. Inevitably, the coupled calculation between MCNP and MCFD is required for system level phenomena such as saturated steady state power and associated overall heat transfer coefficient. The coupling methodology for the current application builds on the method described in the associated research report [12].The calculation steps are summarized below with a logical diagram of the coupling procedure in Figure 8.

- Set up an initial cold start operating condition and baseline solution vessel geometry.
- Evaluate the criticality of the baseline solution vessel by conducting Kcode calculation and confirm the calculated keff is sufficiently close to the desirable value (i.e. 0.98)

- Perform MCNP-run#1 to calculate the power profile at the cold start condition (20C, 140g-U/L)
- Map the output result of MCNP-run#1 into MCFD-run#1 using a UDF function of volumetric energy generation and bubble generation
- Run MCFD-run#1 to achieve the steady state multiphase natural circulation characteristic and extract the temperature profile and volume averaged solution density profile
- Evaluate the updated system power by comparing to the previous power. If the power is not converged, update the MCNP input with the updated temperature card and solution density information.
- Proceed with this coupled calculation (MCNP+MCFD-loop) until the power is saturated.

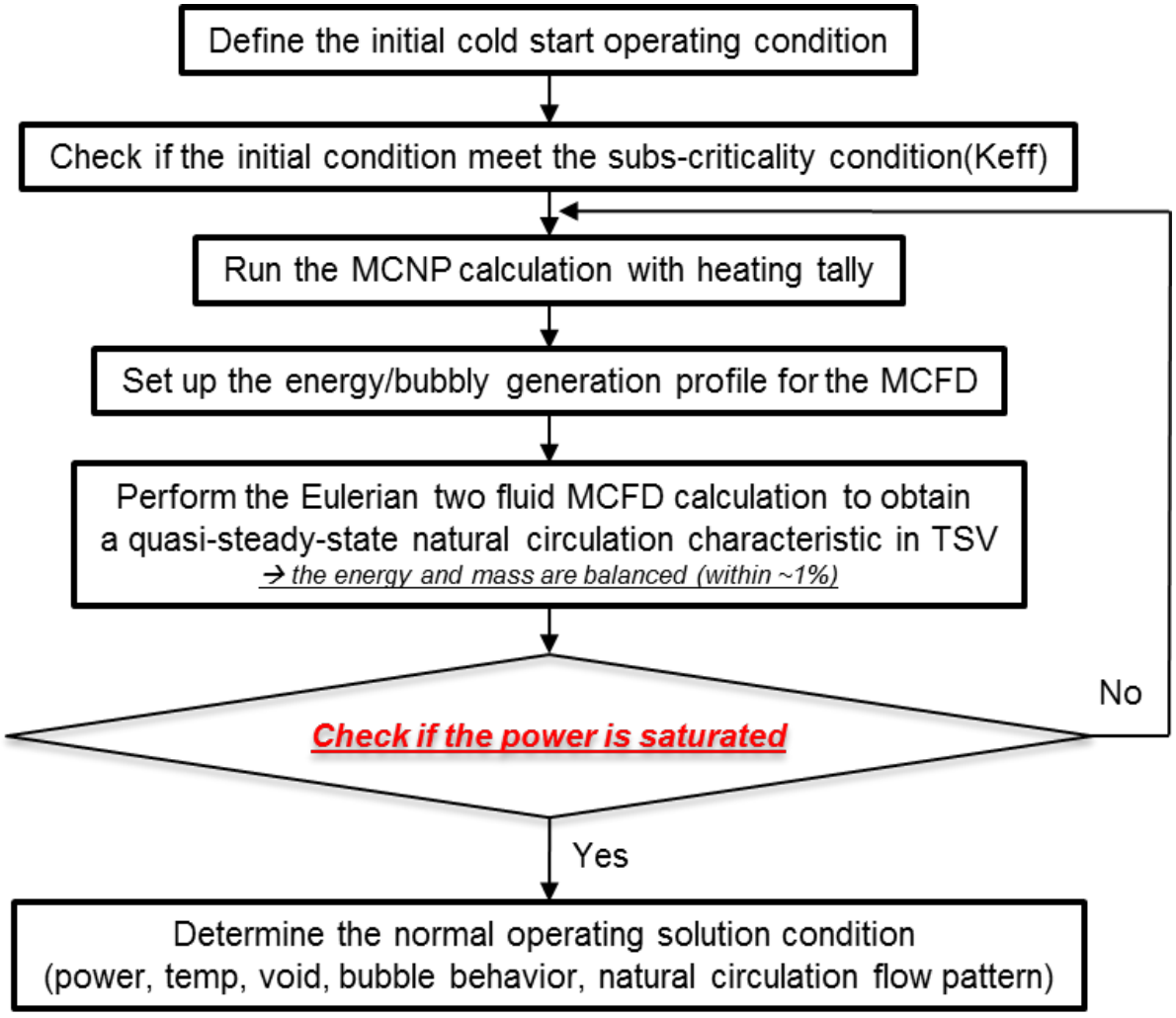

Figure 8 Logical flow chart for the proposed MCFD+MCFD coupling procedure

It should be noted that the coupling methodology described above does not account for dynamic solution height adjustment while the consecutive coupling procedure progresses. Without consideration of height adjustment in the coupled calculation, the actual power could be under-predicted due to some amount of fissile material loss while updating the density in the MCNP calculation. In addition, the volume averaged density calculation for the whole solution as a single unit cell probably results in a less representative power profile compared to a solution volume featuring a varying density profile. These effects are further investigated by improving

the current coupling methodology with a) dynamic height adjustment, and b) a multi-cell approach in chapter 5.

4. Coupled simulation results

4.1 Case study overview

To assess the maturity of the proposed coupling methodology, four different neutron source cases for the baseline solution vessel configuration are investigated in the current study. The baseline solution vessel configuration and the consistent cold start condition (20C, 140g-U/L) are used. The test matrix with initial system parameters are summarized in Table 3. Each corresponding source neutron strength is selected to provide initial power density values from 0.51 KW/L to 3.05 KW/L. As mentioned in the previous section, the bubble generation rate is estimated based on the power profile. In the coupled simulation perspective, the most challenging and least validated estimation applied for the current simulation is the bubble diameter prediction correlation. The correlation between bubble diameter and power density was developed from analysis of data provided in previous researchers' reports [7, 8] and bubble sizes measured in an experiment performed at Argonne Nat'l Lab [9]. The function used to estimate the bubble size (in mm) from the power density (in kW/L) is: $dia[mm] = 0.625 \times power\ density\left[\frac{Kw}{L}\right] + 0.11$. It should be noted that the correlation is developed within a limited power density range, up to 1.55 KW/L, so extrapolated bubble diameters were used for the high power density calculations, such as CASE4 with 3.05KW/L.

Each coupled calculation (MCNP+MCFD) was carried out with at least five iterative loops. The total computing time for a fully coupled calculation for each case is 5 days. The majority of computing time is consumed by the MCFD session (20 hours is needed for each multiphase thermal hydraulic calculation). The cluster specification used is listed below.

- 4 node-cluster with Intel Xeon V1 processor (3.2 GHZ, 8-cores): 32 cores used in total
- 16GB of RAM for each node: 64GB used in total
- Parallel computing with Intel/ Open MPI architecture

Table 3 Detailed Case study matrix with associated initial parameters

	Source Neutron strength [#/s]	**Initial power density [KW/L]**	**Initial Bubble diameter [mm]**	**Initial Bubble generation rate [kg/s]**
CASE 1	1.458e14	0.51	0.431	1.77e-5
CASE 2	2.916e14	1.02	0.763	3.54e-5
CASE 3	5.832e14	2.04	1.4	7.09e-5
CASE 4	8.745e14	3.05	2.1	1.06e-4

The primary results and variables monitored from each solver are listed

- MCNP
  - Radially averaged energy deposition profile (i.e. Q(r,z))
  - Flux tally and heating tally
- MCFD
  - Temperature and void distribution in the solution
  - Energy and gas generation profile
  - Bubble (vapor phase) velocity (i.e. bubble rising velocity)
  - Liquid velocity (i.e. natural circulation pattern)
  - Degassing rate calculation

The ultimate objective of case study in Table 3 is to predict a steady state power level and overall heat transfer coefficient (HTC) for the solution vessel component and to assess the applicability of the proposed HTC in the system code (e.g. SimApp) for the solution vessel application.

4.2 Detailed calculation procedure and associated analysis for CASE1 study

In this session, we report the results of the case 1 coupled calculation that starts from the cold-start condition (20°C, 140g-U/L) at the neutron source of 1.458e-14 [s^{-1}]. The initial power profile is calculated at the cold start condition (MCNP-run#1). The volumetric energy generation and correlated radiolytic gas generation rate are used in the MCFD-run#1 simulation to calculate the steady state thermal hydraulic results such as temperature and void fraction profile.

As mentioned in the previous section, the pseudo transient approach is utilized to calculate the steady state natural circulation behavior in the solution. Proper time scale selection in the pseudo transient approach is vital to capture the associated physics in the flow solver for the free convection flow analysis case. In the current application, the time scale for the simulation can be estimated from the bubble rising velocity that is approximated from the degassing mass flow rate and the degassing surface area. For the case 1 condition, the proper time scale for the MCFD simulation is set to be less than 0.015s. To evaluate the selected time scale's feasibility for the current thermal hydraulic simulation, the energy and mass values are monitored and their conservation is confirmed at the end of the simulation. The total number of iterations for each converged MCFD simulation is 100K, which ensures that the simulations sufficiently capture a reliable multiphase natural convection physics. The energy and mass balance for the MCFD-run#1 are shown in Figure 9. As expected, the energy loss by cooling surfaces and the mass loss from the degassing top surface are identical to the energy and mass input calculated from the MCNP-run#1.

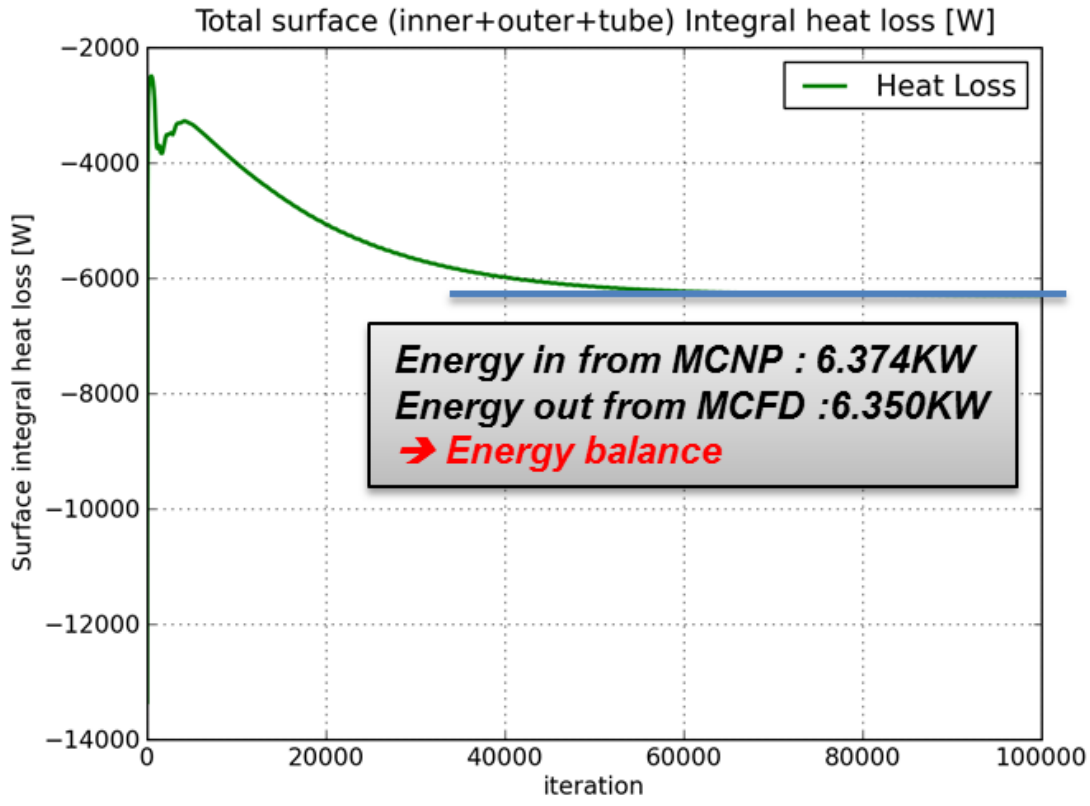

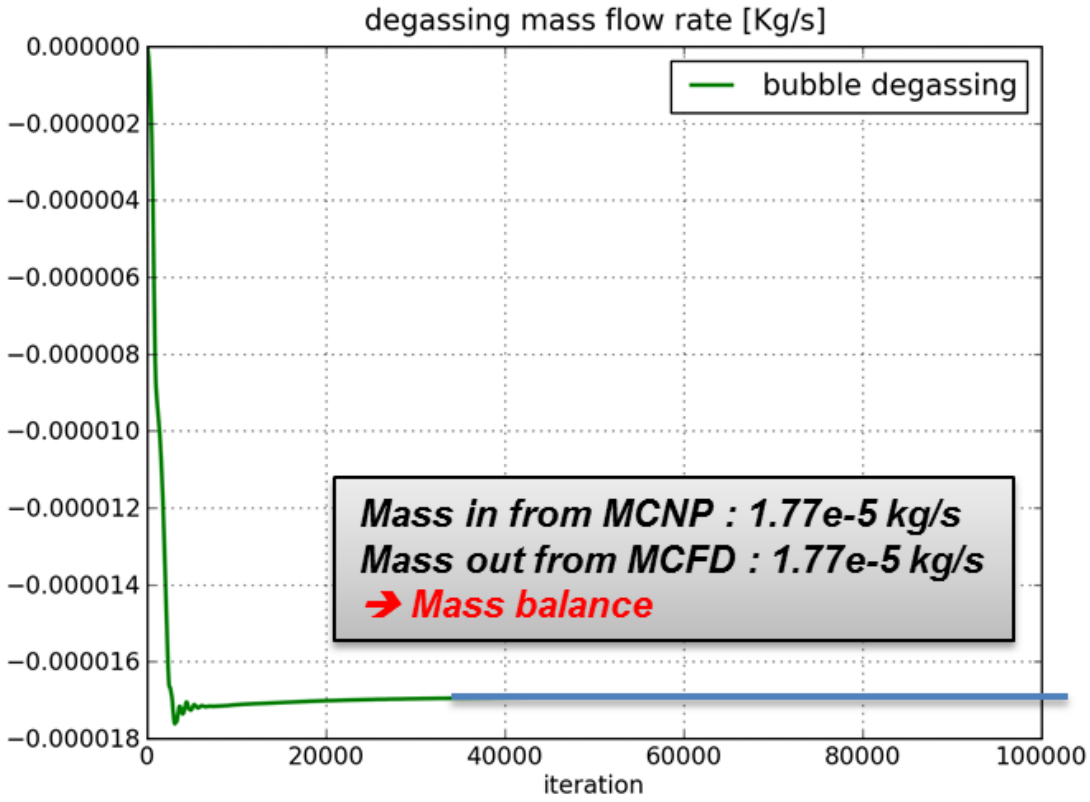

Figure 9 Energy and Mass balance check in coupled calculation

A saturated MCFD simulation (i.e. MCFD-run#1) produces the updated solution temperature and density profiles for the next MCNP calculation (i.e. MCNP-run#2). The associated temperature card and density profile in the solution material card are accordingly updated. Due to the nature of the multiphase (liquid phase and vapor phase) solution, the appropriated definition of density for Uranyl Sulfate should account for the solution temperature and void fraction (VF) using the following equation:

$$Solution\ density = \rho_{fuel} \times VF_{fuel} + \rho_{gas} \times VF_{gas} \qquad \text{Eq-1}$$

The updated temperature and density information is fed into the MCNP-run#2 to progress the consecutive coupled calculation. This series of loop (MCNP-run#1 and MCFD-run#1) illustrate how the neutron calculation affects the multiphase thermal hydraulic behavior and vice versa as shown in Figure 10.

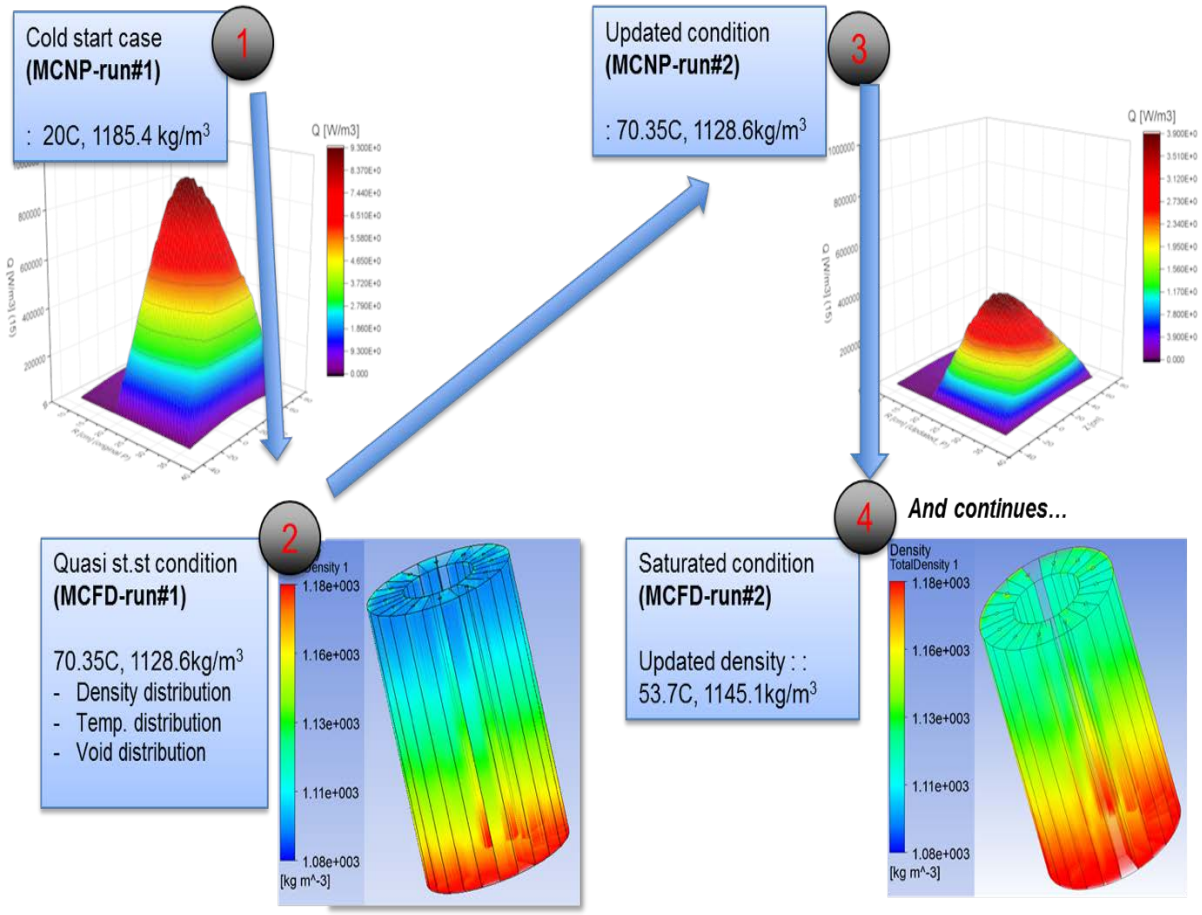

Figure 10 A graphical demonstration of consecutive coupled MCNP+MCFD calculation

Furthermore, the MCFD simulation provides a deeper insight into the multiphase thermal-hydraulic behavior such as qualitative bubble rising pattern, quantitative rising velocity and natural circulation flow motion within the solution vessel. Figure 11 demonstrates both the detailed multiphase flow motion and the calculated velocity information by illustrating the vapor phase degassing physics and liquid phase natural circulation, repsetively. This type of analysis provides useful insight for the cooling design and the cooling structure configrations. For example, the bubble rising pattern is concentrated along tube channel at the center, while negligible upward flow at the inner and outer channel is observed. A more complex liquid phase natural circulation pattern is found with a relatively slow velocity compared to the vapor phase. Most interestingly, a relatively strong (i.e. faster liquid circulating velocity) natural circulation leaning toward the inner channel is observed with maxium liquid velocity. With this in mind, an improved natural circulation heat transfer mechanism by different cooling configuration or solution aspect ratio can be further investigated using the MCFD analysis. Unfornately, this report only focuses on the maturity of the coupled calculation method and the predicted steady state power and generalization of a heat transfer coefficient. However, the analysis demonstrated here opens a ponteial research path for the improved solution vessel design as a future study.

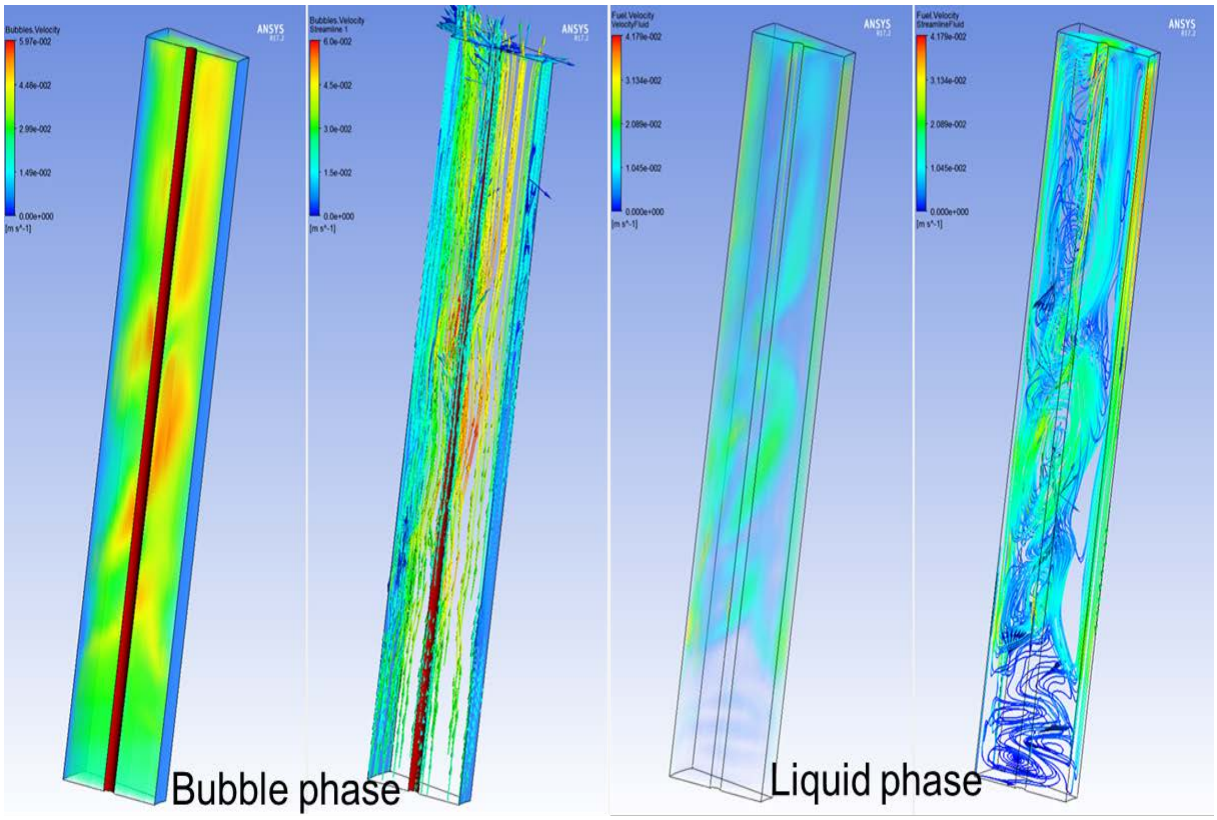

Figure 11 Velocity contour and streamline for bubble phase and liquid phase

Figure 12 shows the convergence of key monitoring parameters in the MCFD calculations including power, temperature, and void fraction. As usual, in a general CFD practice, the energy equation takes a substantial amount of simulation time (i.e. 100K iterations) to obtain a reasonable saturated pattern, unlike mass continuity, which converged after 10K iterations. However, it is critical to check both energy and mass balance for high fidelity HTC correlation development. In this simulation, consecutive coupled calculations ran for at least 5 loops or less than 1% power deviation between the previous calculation and present calculation. For case 1 study, the power is saturated at 3.1KW, which is less than 50% of the initial power calculation from MCNP-run#1. The saturated steady state operating temperature of the solution vessel is predicted to be 56.4°C which is well below the boiling temperature of uranyl sulfate solution. The volume averaged void fraction of the system at the steady state condition is estimated to be 2.3%.

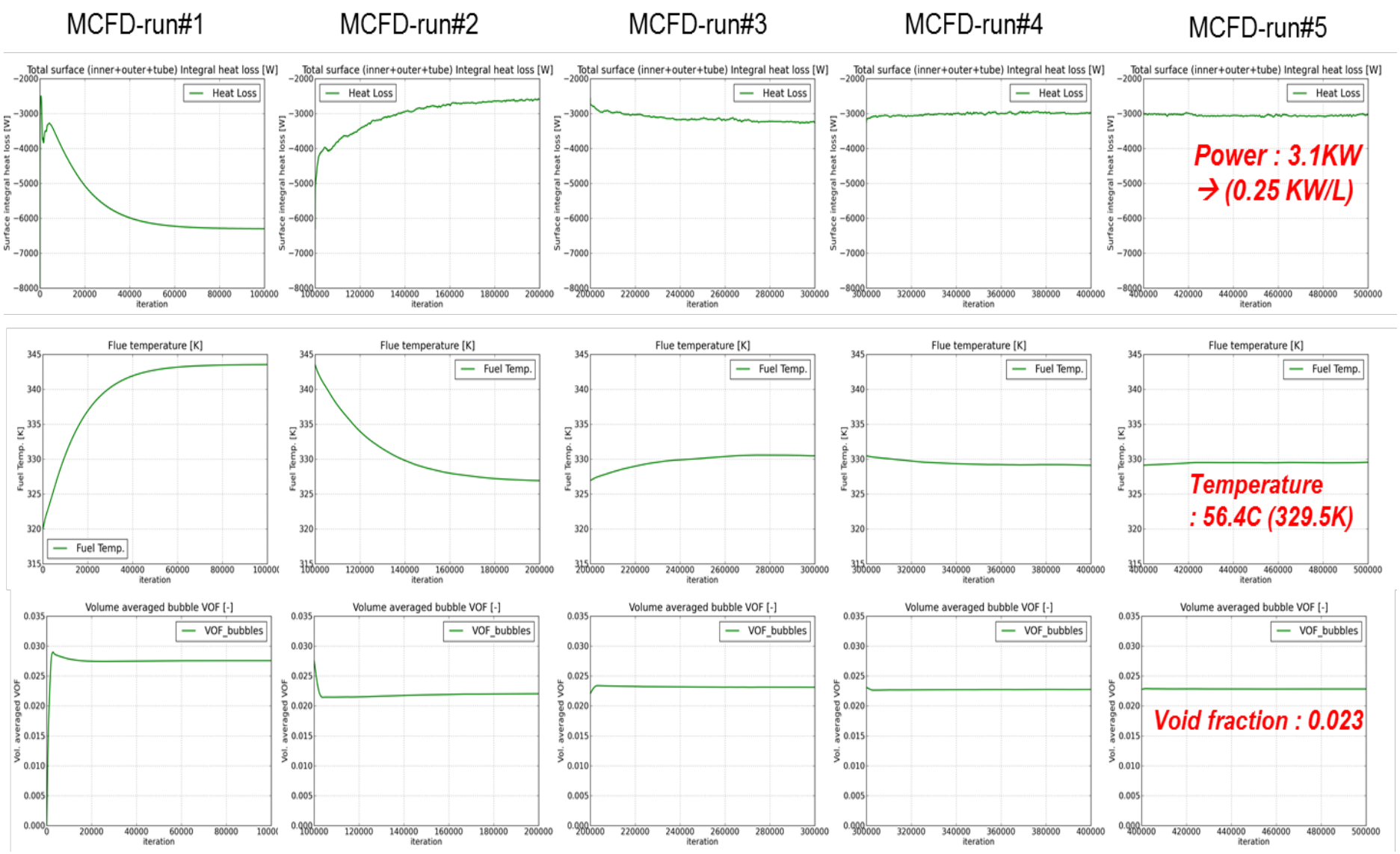

Figure 12 Saturated system power, solution temperature and void fraction convergence as consecutive MCFD simulation progresses in case 1

Extrapolating of power prediction after 5 consecutive calculations led to a postulated normal operating power at steady state condition as shown in Figure 13. It is an interesting finding that the postulated normal operating power with the given initial neutron source leads to about half of the initial power value from the cold start condition. The discrepancy between the initial power calculation and the steady state power calculation was a result of the coupled physics in the generic solution vessel system. Quantifying the power reduction mechanism and identifying the postulated steady state power value is imperative to the design of a generic solution vessel for a Moly99 production application.

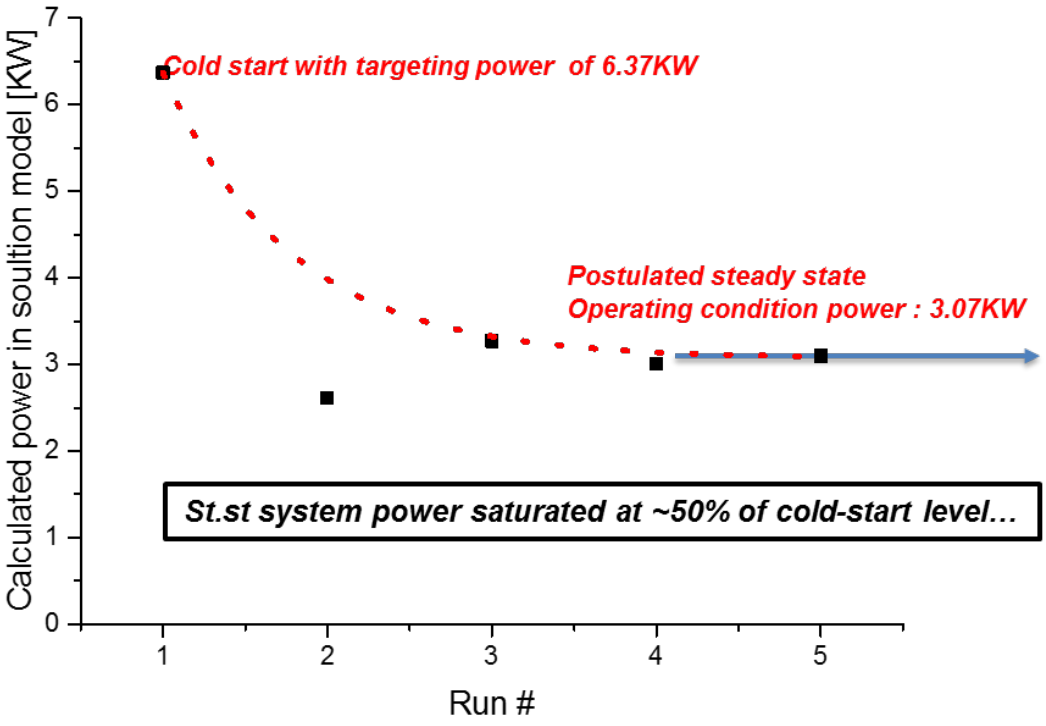

Figure 13 Solution power along with consecutive MCFD runs.

The overall heat transfer coefficient for case1 is calculated using a lumped approach as follows.

$$HTC = \frac{Q_{st.st}}{A \times \Delta T} = \frac{3070}{0.17761 \times 30.68} = 563.0894 \left[\frac{W}{m^2 K}\right] \quad \text{Eq-2}$$

where, $Q_{st.st}$ is the calculated steady state power from coupled calculation, A is the total area of the cooling channels (tube, inner channel, and outer channel), and ΔT is the temperature difference between the averaged bulk fluid temperature and averaged cooling wall temperature.

Alternatively, the MCFD simulation can plot the local HTC contour over the whole cooling surface. The HTC value is a local parameter for the thermal hydraulic application. So visualization of the HTC value over the cooling surface can provide useful insight for cooling efficiency and cooling design improvement. As shown in Figure 14, the local HTC value varies from 250 ~ 2480 W/m^2-K over the cooling surface. As expected, a high local HTC value is found at the top, where a large lateral temperature change (i.e. bulk to near wall temperature) is observed in the MCFD simulation. Nevertheless both lumped approach based HTC calculation and MCFD based HTC calculation demonstrate similar predicted values. In this report HTC values from the lumped approach are documented and used for the HTC correlation development.

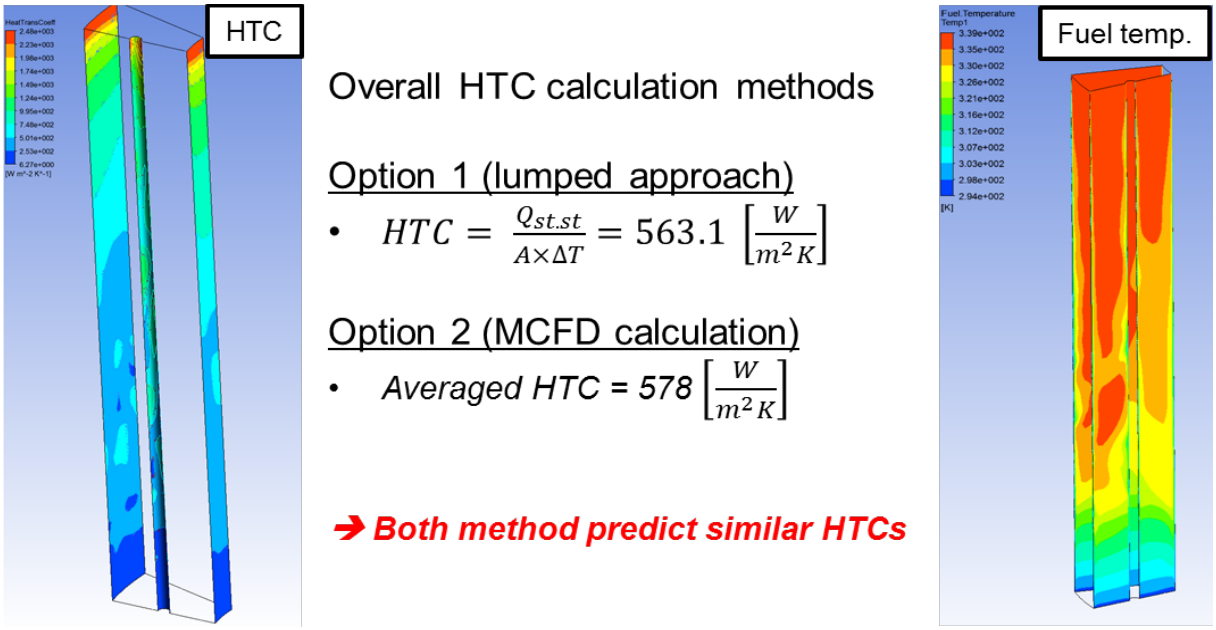

Figure 14 Calculation methods for overall HTC of naturally circulating solution

4.2 The effect of initial neutron source strength on power and HTC calculation

After a successful coupled calculation is demonstrated for CASE1, we further explore this multi-physics calculation with a range of initial neutron source strengths. The baseline solution vessel geometry and cold start operating condition are fixed. 5 consecutive coupled calculations for each case are simulated, and the final power is saturated with less than 5% deviation. 4 test cases with initial source neutron and calculated power levels are listed below

- Case 1: Source Neutron (SN) = 1.458e14 s^{-1} → initial power = 6.37KW
- Case 2: Source Neutron (SN) = 2.916e14 s^{-1} → initial power = 12.7KW
- Case 3: Source Neutron (SN) = 5.832e14 s^{-1} → initial power = 25.5KW
- Case 4: Source Neutron (SN) = 8.754e14 s^{-1} → initial power = 38.2KW

Figure 15 represents comprehensive results from the coupled calculations (MCNP+MCFD) with 4 different source neutron values. All cases start from the fixed cold start condition and eventually reach the steady state power operating condition. The final saturated operating solution temperature for all 4 cases is found to be less than boiling point (assumed to be 100°C) which ensures the thermal properties developed for the current study are valid for this particular application. Similar to the convergence shown in Figure 13, all multi-physics simulation performed for Case 2, 3, and 4 also converged to the final saturated value after a few oscillatory fluctuations in the power results. It is observed that a high power case (CASE4, high source neutron) takes more iterative coupled calculations than a low power case (CASE1, low source neutron). At every run of MCFD simulation, a volume rendered density profile in the full geometry of the solution vessel is reported to visualize how the two phase thermal hydraulic results in terms of temperature and void fraction are stabilized in the coupled calculation (Figure 15). Note that the legend value for the density profile is optimized for the CASE-1-MCFD-run#1 and identical legends are used for the rest of the contour plots to make a clear comparison. The transparent density images in the higher power cases represent a density in those areas that is less than 1085 kg/m^3 due to high temperature and high void fraction.

CASE-1 (SN=1.458e14s^{-1})	Run#1 (cold start)	Run#2	Run#3	Run#4	Run#5
MCNP ***Cold start condition*** ***(20C, 1185.4 kg/m3)***	Input: 20C, 1185.4 kg/m3 Output: 6.37KW	Input: 70.3C, 1128.6kg/m^3 Output: 2.61KW	Input: 53.7C, 1145.1kg/m^3 Output: 3.27KW	Input: 57.3C, 1141.8kg/m^3 Output: 3.01 KW	Input: 55.9C, 1143.0kg/m^3 Output: 3.10 KW
MCFD Predicted normal operating condition ***(56.4C, 1142.6kg/m^3)***	Input: 6.37KW profile Output: 70.3C, 1128.6kg/m^3	Input: 2.61KW profile Output: 53.7C, 1145.1kg/m^3	Input: 3.27KW profile Output: 57.3C, 1141.8kg/m^3	Input: 3.01 KW profile Output: 55.9C, 1143.0kg/m^3	Input: 3.10 KW profile Output: 56.4C, 1142.6kg/m^3

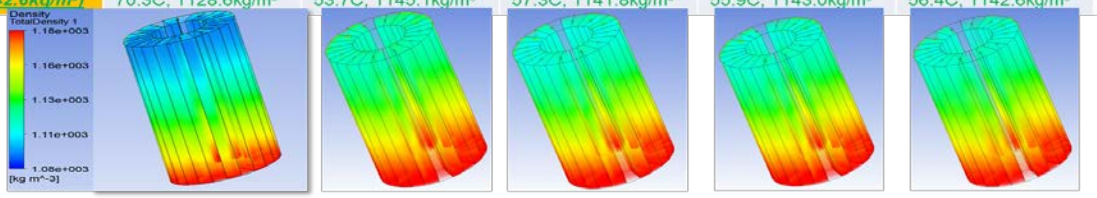

CASE-2 (SN=2.915e14s^{-1})	Run#1 (cold start)	Run#2	Run#3	Run#4	Run#5
MCNP ***Cold start condition*** ***(20C, 1185.4 kg/m3)***	Input: 20C, 1185.4kg/m^3 Output: 12.75KW	Input: 97.7C, 1103.0kg/m^3 Output: 4.09KW	Input: 61.9C, 1137.5kg/m^3 Output: 5.86KW	Input: 68.4C, 1111.1kg/m^3 Output: 5.39KW	Input: 66.8C, 1132.6 kg/m^3 Output: 5.51KW
MCFD Predicted normal operating condition (67.3C, 1132.1kg/m3)	Input: 12.75KW profile Output: 97.7C, 1103.0kg/m^3	Input: 5.09KW profile Output: 61.9C, 1137.5kg/m^3	Input: 5.86KW profile Output: 68.4C, 1131.1kg/m^3	Input: 5.39KW profile Output: 66.8C, 1132.6kg/m^3	Input: 5.51KW profile Output: 67.3 C, 1132.1kg/m^3

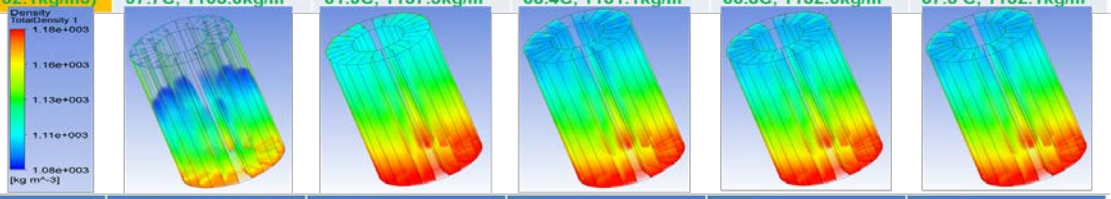

CASE-3 (SN=5.83e14s^{-1})	Run#1 (cold start)	Run#2	Run#3	Run#4	Run#5
MCNP ***Cold start condition*** ***(20C, 1185.4 kg/m3)***	Input: 20C, 1185.4kg/m^3 Output: 25.5KW	Input: 166.8C, 1088.7kg/m^3 Output: 7.25KW	Input: 73.7C, 1125.8kg/m^3 Output: 10.15 KW	Input: 86.1C, 1113.1kg/m^3 Output: 8.98 KW	Input: 80.6C, 1118.1kg/m^3 Output: 9.55 KW
MCFD Predicted normal operating condition (83.3C,1116.0kg/m^3)	Input: 25.5KW profile Output: 166.8C,1088.7kg/m^3	Input: 7.25KW profile Output: 73.7C, 1125.8kg/m^3	Input: 10.15KW profile Output: 86.1C, 1113.1kg/m^3	Input: 8.98W profile Output: 80.6C, 1118.1kg/m^3	Input: 8.98W profile Output: 83.3C, 1116.0kg/m^3

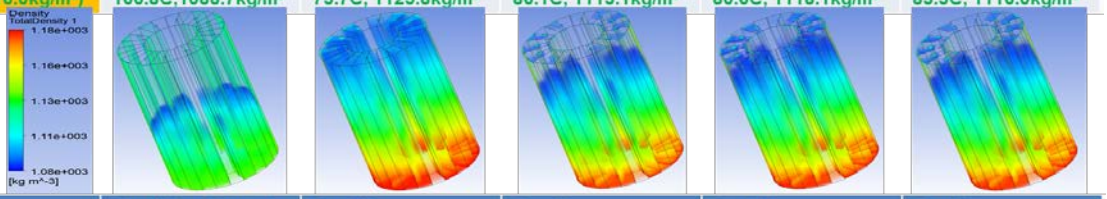

CASE-4 (SN=8.745e14s^{-1})	Run#1 (cold start)	Run#2	Run#3	Run#4	Run#5
MCNP ***Cold start condition*** ***(20C, 1185.4 kg/m3)***	Input: 20C, 1185.4 kg/m^3 Output: 38.2KW	Input: 224.5C,1073.7 kg/m^3 Output: 9.59KW	Input: 83.7C, 1115.7 kg/m^3 Output: 13.8KW	Input: 103.8C, 1101.2kg/m^3 Output: 11.9KW	Input: 94.1C, 1105.7kg/m^3 Output: 12.5KW
MCFD Predicted normal operating condition (96.9C,1103.7kg/m^3)	Input: 38.2KW profile Output: 224.5C,1073.7kg/m^3	Input: 9.59KW profile Output: 83.7C,1115.7kg/m^3	Input: 13.8KW profile Output: 103.8C,1101.2kg/m^3	Input: 11.9KW profile Output: 94.1C,1105.7kg/m^3	Input: 12.5 KW profile Output: 96.9C,1103.7kg/m^3

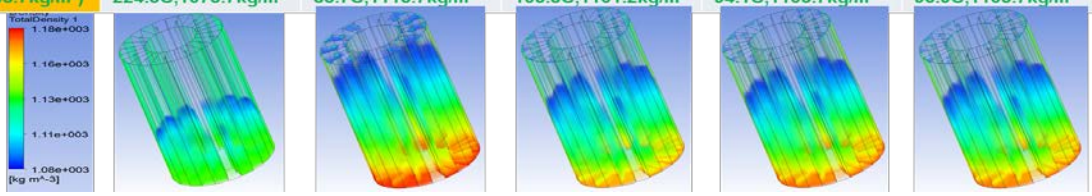

Figure 15 A summarized result of iterative multi-physics calculation with density profile

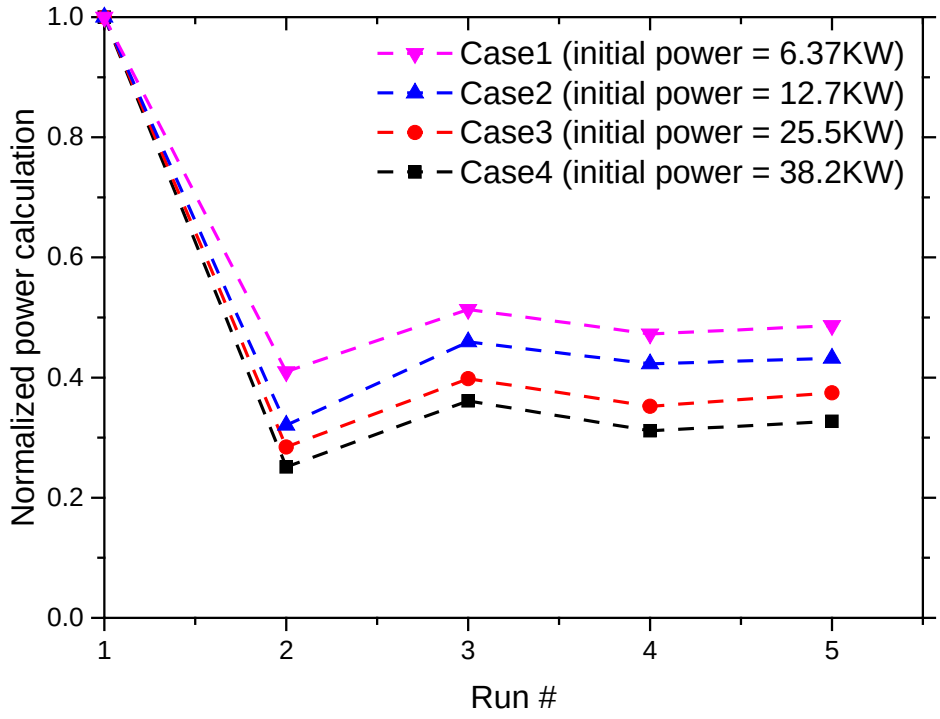

Figure 16 Normalized calculated power monitor over 5 iterative MCNP+MCNP simulations

The saturated power results from the coupled calculations are normalized based on the initial power value at each case study, and the trends of the power saturation as the coupled calculation progressed are illustrated in Figure 16. A few key observations are summarized below.

- The final saturated power from the coupled simulation becomes less than 48% of initial power level.
- The power reduction rate is more pronounced when the initial power is higher (i.e. CASE4, less than 32% of initial power)
- The predicted steady state power density (i.e. the calculated power / the solution volume) varies from 0.25 KW/L (Case1) to 1.05KW/L (Case4)
- For the high power cases, additional iterative coupled calculations are recommended, and the thermal property correlations used in MCNP and MCFD need to be doubled-checked, since the operating temperature could be beyond the boiling condition in some regions.

HTCs for four cases are evaluated using the lumped approach method mentioned in the previous chapter. A generalization of the HTC at different steady state power density is plotted in Figure 17. With an applicable range of power density from 0.25KW/L to 1KW/L, an HTC correlation for the solution vessel is proposed bleow.

$$HTC\left[\frac{W}{m^2K}\right] = 581.36\ln(power\ density\left[\frac{KW}{L}\right]) + 1359 \qquad \text{Eq-3}$$

Furthermore, the comparison between the proposed correlation from the current study and the used correlation in the system analysis code will be further investigated, and an assessment of the proposed HTC correlation with different solution vessel configurations (cooling

configuration and solution vessel aspect ratio) can be performed in the following work.

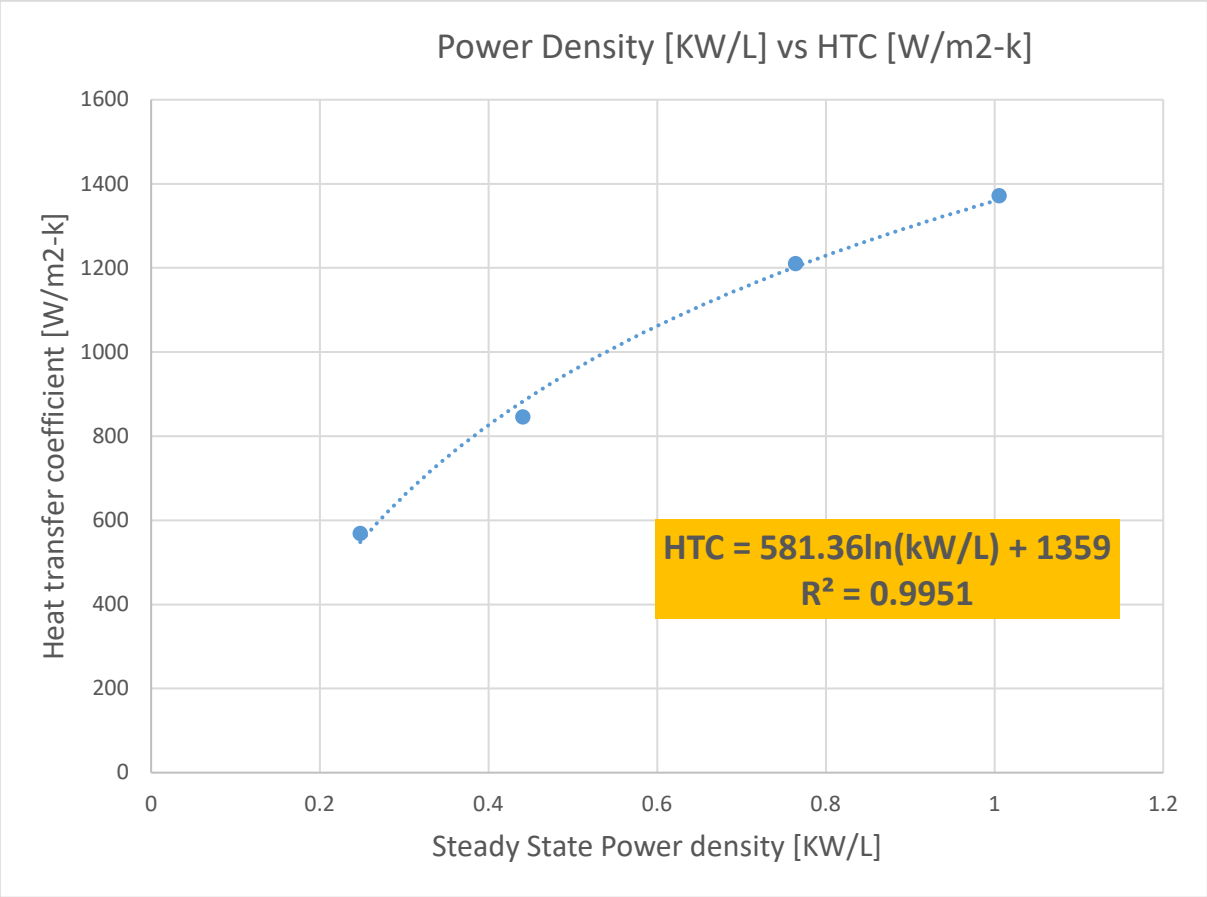

Figure 17 HTC correlation for the solution vessel with power density

5. Improved coupled calculation methodology

While developing and demonstrating the current coupled multi-physics methodology, a few improved coupled calculation methods have been discussed to better capture non-trivial physics that were neglected in the original coupled calculation method. Two improved methods will be discussed in this section. Those methods include dynamic height adjustment and multi-cell approach for the solution vessel model.

5.1 Improvement-1: Height adjustment

In the coupled calculation procedure, the density of Uranyl Sulfate kept changing as the thermal hydraulic calculation by MCFD updated the temperature and void profile. However, without updating the solution height, the updated density with fixed solution volume could lead to the underestimation of the mass of fissile material in the solution vessel, which results in the under-prediction of the power and HTC. This limitation can be resolved by dynamically updating the solution height which represents the thermal expansion behavior in the solution and maintaining the total fission material constant during iterative coupled calculations. The updated height is estimated based on the volume-averaged density change in the MCFD calculations.

$$V_1\rho_1 = V_2\rho_2 \ (mass\ conservation) \qquad \text{Eq-4}$$

$$\therefore H_2 = H_1\frac{\rho_1}{\rho_2} \qquad \text{Eq-5}$$

Case 1 was simulated again with the height adjustment approach, and the solution height change along with the progression of the coupled calculation is illustrated in Figure 18. The final solution height (1.093m) is increased by 3.8% compared to the original calculation with constant height (1.053m).

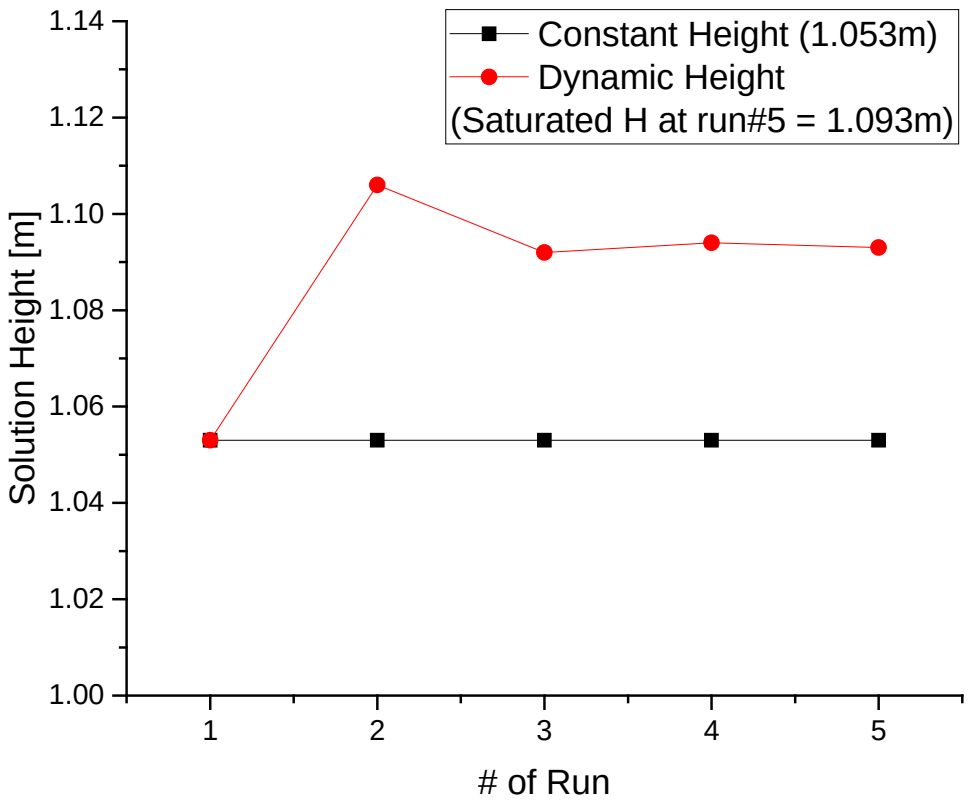

Figure 18 Solution Height monitor with dynamic height adjustment method

The results of the saturated MCFD calculation with height adjustment method were post-processed to extract the power level, operating temperature, volume averaged void fraction, and degassing mass flow rate and compared to the original run (Case1). The temperature, void fraction, and degassing mass flow rate results are similar to the original simulation. However, the power is predicted to be a higher value in the improved methodology (i.e. original CASE1 calculation: 3.1KW, CASE1 with height adjustment 3.28KW). It is confirmed that the mass conservation achieved by updating the solution height leads to a higher power prediction which should be closer to the exact value of the system power at the steady state condition.

5.2 Improvement-2: Multi-cell approach for the solution vessel

Another possible limitation in the current coupling methodology would be the lack of a realistic non-uniform density profile for the solution in the MCNP calculation. The original coupling approach assumes that the solution in the vessel can be represented as a unit-cell of uniform density, which does not represent the real vertically-varying density profile. Simulations have revealed higher density regions at the bottom and lower density regions at the top of the solution. Thus, we developed a multi-cell approach for the solution vessel model for both MCNP and MCFD. Graphical representations for the MCNP model illustrated in Figure 19 effectively describe the different concepts of the MCNP modeling (unit-cell approach vs. multi-cell approach) and the corresponding heating tally based energy deposition calculations.

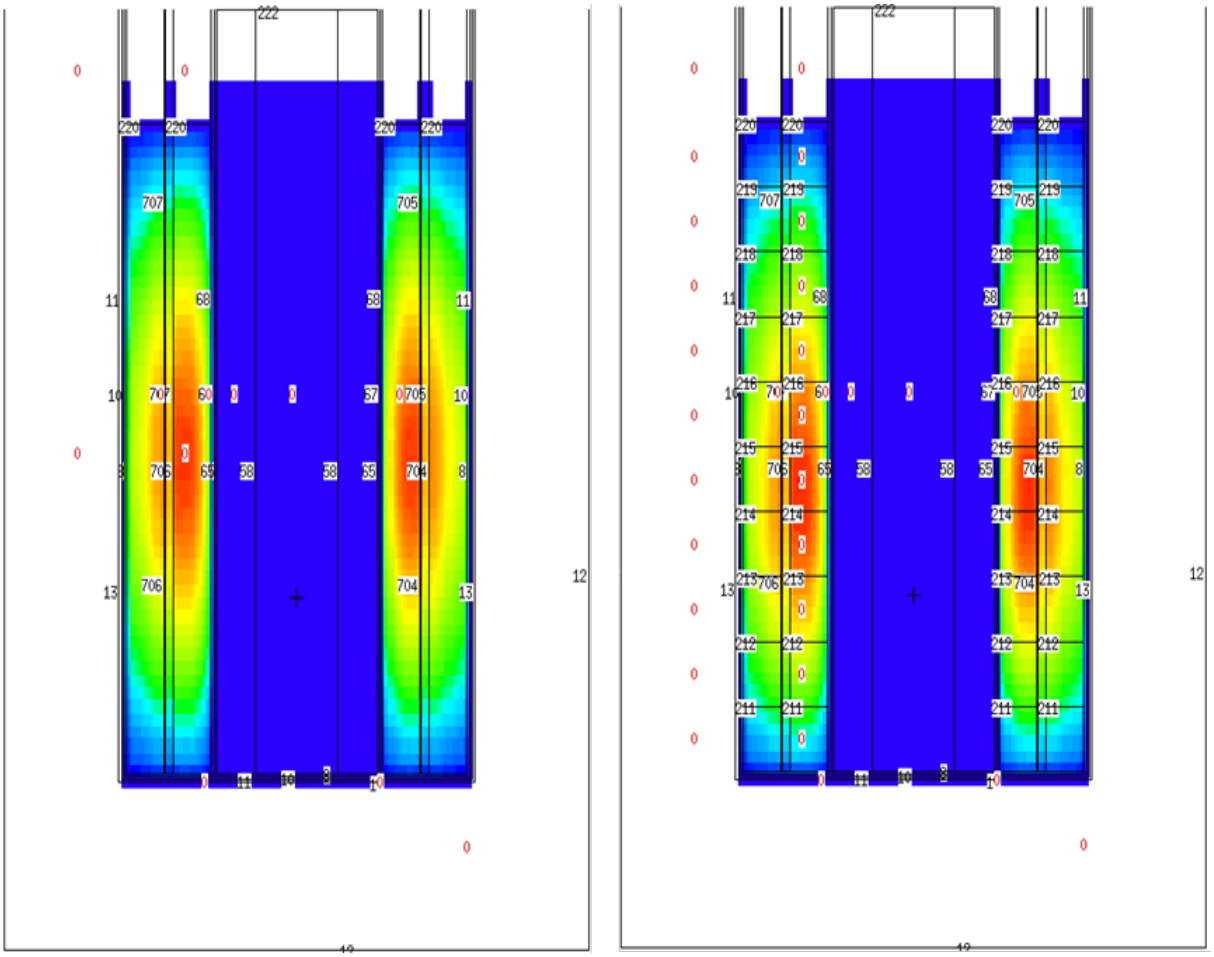

Figure 19 Energy deposition comparison between single-cell and Multi-cell at the converged calculations

The solution vessel is segmented into 10 cells in the multi-cell approach with a non-uniform density profile calculated from the MCFD. The left plot in Figure 19 resulted from the single-cell calculation, and the right plot resulted from the multi-cell approach. With the same volume averaged density condition, the Multi-cell approach with non-uniform density profile demonstrated a relatively higher maximum peak energy deposition with a slightly down-shifted power profile. This comparative result indicates that the implementation of non-uniform density could cause different power behavior and thermal hydraulic response compared to the original volume-averaged single density approach.

To implement the multi-cell approach in the MCFD, the fluid domain is also accordingly segmented to match the MCNP model. The segmented density and temperature results are monitored and plotted in Figure 20. Segment-1 represents the bottom cell of the solution vessel, which is expected to be lowest temperature and highest solution density, and segment-10 is the top cell of the solution vessel with highest temperature and lowest solution density. Note that this multi-cell based MCFD simulation requires additional computing cost due to the additional variables to monitor and store in the data output files. Per the current practice, the simulation time for the multi-cell calculation tripled compared to the original method.

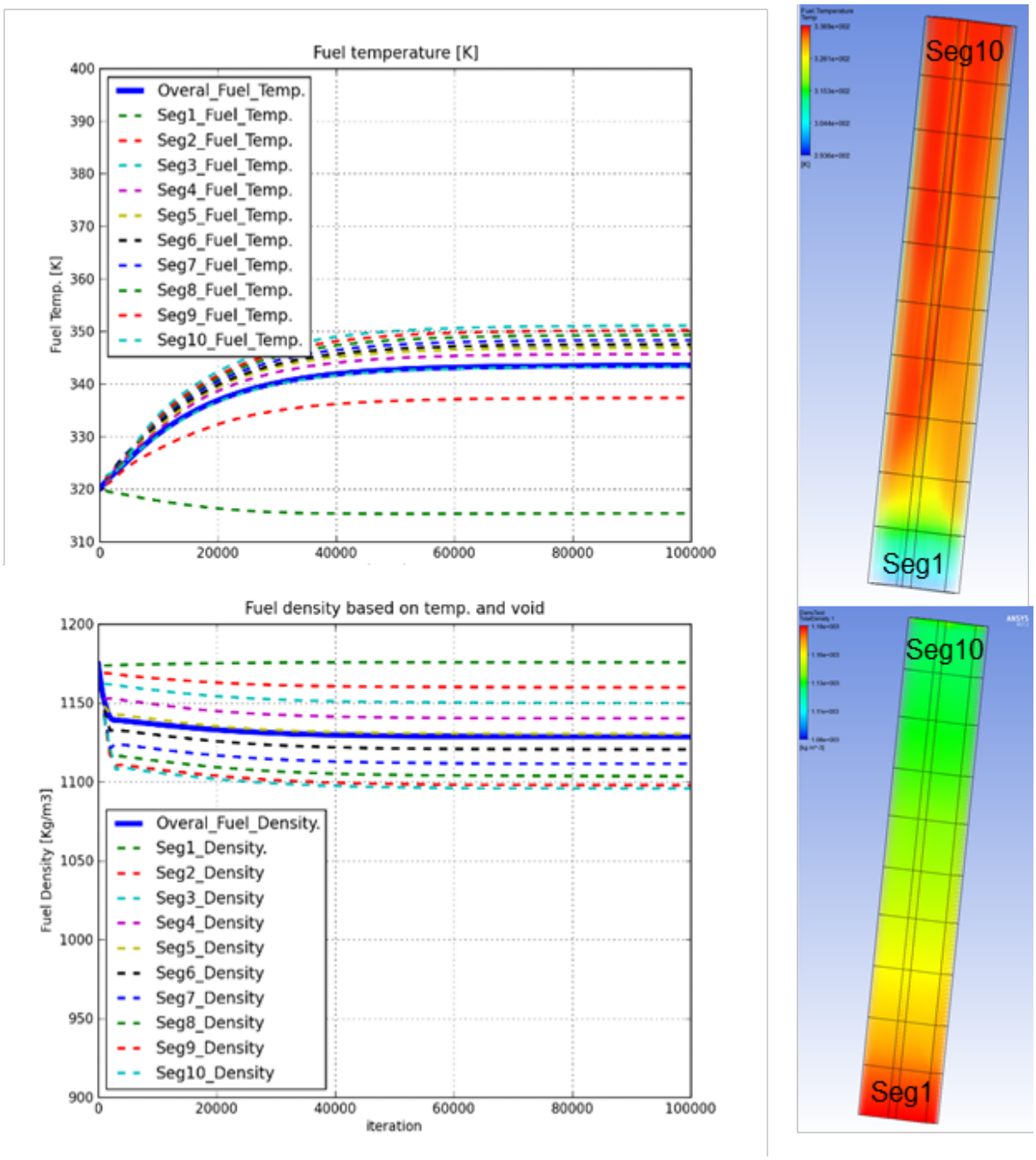

Figure 20 Segmented fuel temperature and density monitoring in multi-cell MCFD

A summarized progress result of the coupled MCNP+MCFD calculations with multi-cell & height change methodology is reported in Figure 21. The final steady state converged solutions (e.g. power, solution temperature, void, degassing mass flow, density) are illustrated and compared to the original method (CASE1) in Figure 22. The key findings observed in the current approach can be highlighted as follows.

- The final height at the saturated power after 5 iterative calculations is saturated at 1.083m, which is a 2.85% increase from the initial solution height.
- The non-uniform density and temperature profiles for the 10-segment solution cell are updated in every step of the iterative calculation in both the MCNP and MCFD models.

- The volume averaged solution temperature for the entire vessel matches the volume averaged temperature for segment 3 in the multi-cell model.
- The volume averaged solution density, accounting for the bubble void fraction, agrees well with the volume averaged density of segment 5.
- The final system power is saturated at 3.63KW, which is 58% of the initial power level at cold start.
- The slip ratio (i.e. the ratio of vapor phase velocity to the liquid phase velocity in temporal and spatial averaged fashion) in the multi-cell approach is notably increased compared to that in the original calculation (Case1). Consequently, the increase in slip ratio leads to the reduction of void fraction and an increased solution density. The relationship between void fraction and slip ratio can be correlated with the following equation [10]. Note that x denotes the quality of two phase flow (i.e. mass fraction between vapor and liquid), and ρ_l, ρ_v represent the density of liquid and vapor phase

$$\alpha\ (\text{void fraction}) = \frac{1}{1+\frac{1-x}{x}\frac{\rho_v}{\rho_l}S(slip\ ratio)} \quad \text{eq-6}$$

- With the assumption that quality and system temperature are similar at the same level of power, the high slip ratio predicted with the multi-cell approach induces a reduced solution void fraction (less pronounced time averaged gas hold-up phenomenon) and results in an increased power prediction compared to the single-cell calculation.
- Ultimately, improved understanding of the multiphase thermal hydraulic parameters such as void, slip ratio, and the bubble size function may improve the accuracy of the steady state power calculation.
- Interestingly, the HTC value calculated with the improved coupled methodology matches very well the proposed HTC correlation in equation 3. Thus, the HTC is considered to be insensitive to the coupled methodology. However, the power prediction at the steady state condition with the improved coupled methodology differed from the original coupled calculation value.
- Last but not least, the steady state power calculation with improved methodology (height adjustment and multi-cell approach) quantitatively predicts a value 18% higher than the original method (no height adjustment and single-cell approach: 3.07KW → height adjacent with multi-cell approach: 3.63KW). In other words, the original coupled calculation methodology under-predicts the steady state power level due to the lack of mass conservation and the simplified uniform density representation in the solution vessel. This under-predictive capacity in the original coupled methodology will directly result in an underestimation of Moly99 production level (i.e. yield performance estimate). Therefore, the improved coupled methodology (dynamic height adjustment and multi-cell approach calculation) is strongly recommended for a high fidelity steady state power calculation.

MCNP+MCFD coupling progress

(Multi-cell+ Height Change)

$$V_1\rho_1 = V_2\rho_2$$
$$(mass\ conservation)$$
$$\therefore H_2 = H_1\frac{\rho_1}{\rho_2}$$

CASE-1 (SN=1.458e14s^{-1})	Run#1 (cold start) Height = 1.053m	Run#2 Height = 1.106m	Run#3 Height = 1.080m	Run#4 Height = 1.087m	Run#5 Height = 1.083m
MCNP ***Cold start condition*** ***(20C, 1185.4 kg/m3)***	Input: 20C, 1185.4 kg/m3 Output: 6.37KW	Input Varying Temp, Den Output: 2.89KW	Input Varying Temp, Den Output: 3.92KW	Input Varying Temp, Den Output: 3.50KW	Input Varying Temp, Den Output: 3.63KW
MCFD Predicted normal operating condition ***(56.9C, 1149.8kg/m^3)***	Input: 6.37KW profile Output: (Varying) 70.3C, 1128.6kg/m^3	Input: 2.89KW profile Output: (Varying) 52.4C, 1155.7kg/m^3	Input: 3.932W profile Output: (Varying) 58.6C, 1147.4kg/m^3	Input: 3.50W profile Output: (Varying) 56.3C, 1150.9kg/m^3	Input: 3.63W profile Output: (Varying) 56.9C, 1149.8kg/m^3

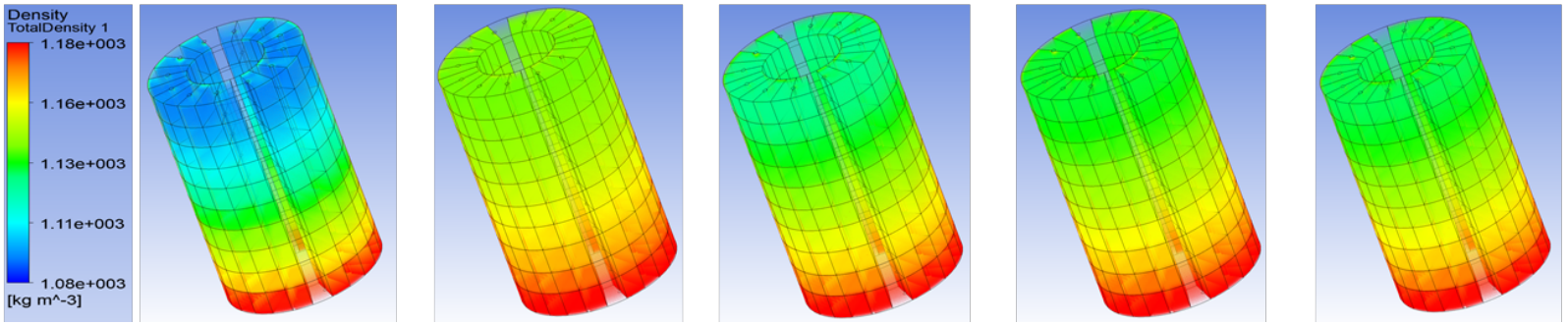

Figure 21 A summarized result of multi-cell approach with height adjustment in each iterative run stage.

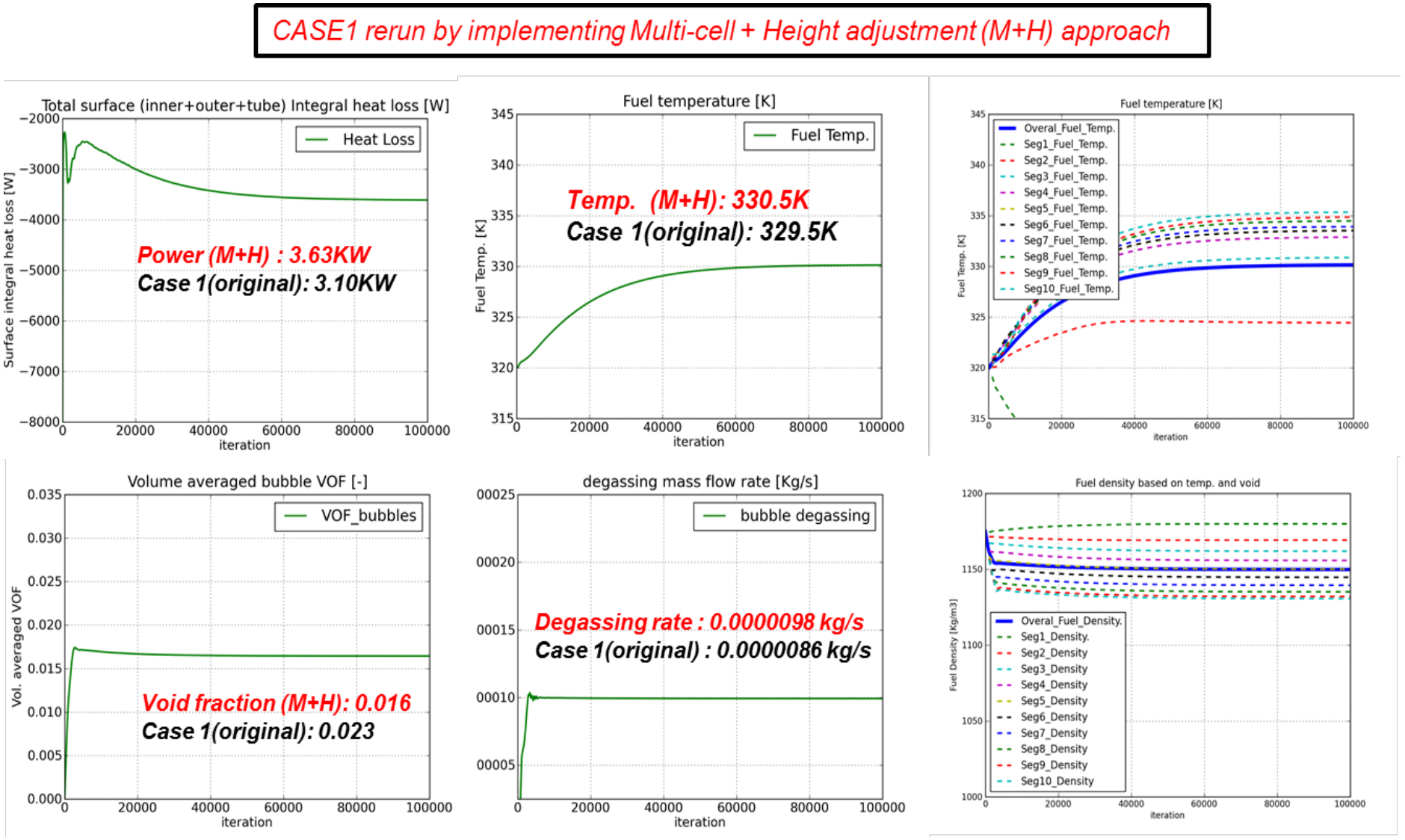

Figure 22 A summarized result of saturated system variables such as power, temperature, void fraction, and degassing rate

6. Summary and future work

The purpose of this study is to demonstrate a fully coupled multi-physics simulation methodology for a generic solution vessel application and to predict the steady state operating power as well as the corresponding heat transfer coefficient at a variety of source neutron strengths. The baseline solution vessel model features three types of cooling structures and a desirable operating condition (e.g. uranyl sulfate solution concentration, cold start keff). A successful coupling between the neutron transfer solver and the multiphase fluid solver provides useful design insight for the generic solution application and an increased understanding of the multi-physics characteristics in the subcritical assembly for a Moly99 production facility design. The main results and key findings can be reiterated as follows:

- Four different source neutron strength cases are selected to perform steady state power and HTC calculations.
- Power predictions and associated HTC calculations are well converged after 5 iterative coupled calculations.
- The HTC values for different power densities are reported, and a generalization of HTC for the proposed baseline solution vessel geometry is produced.
- The original coupled calculation methodology is incrementally improved by implementing concepts to represent a more realistic system. Two improved methodologies (e.g. dynamic height adjustment and multi-cell approach) and associated results are reported, and comparisons to original calculation results are addressed with physical explanations.

Further improvements relating to the current study should be investigated by focusing on the following research items. In particular, another (maybe most important) question for future work would be how to validate the numerical methodology developed for a subcritical solution vessel application with corresponding experimental measurement or system level code analysis.

- Evaluate the heat transfer coefficient of the cooling channels by conducting an analysis of a separate conjugate heat transfer model.
- Perform a series of transient analyses on a generic solution vessel using SimApp and conduct a comparative study between the system code and the multi-physics calculations for various scenarios.
- Build a Python script for automating the coupled calculation procedure.

The authors gratefully acknowledge the help of Greg Dale with the calculation of the neutron source profile used in this analysis. His calculation description is presented in Appendix A.

7. References

1. Paula Gould, “Medical isotope shortage reaches crisis level” *Nature 460, 312-313 (2009)*, doi:10.1038/460312a.
2. IAEA Nuclear Energy series, “Non-HEU production technologies for molybdenum-99 and Technetium-99m” IAEA No. NF-T-5.4, 2013.
3. The Densities of Uranyl Sulfate Solutions between 20° and 90°C, Mound Laboratory, MLM-728, Oct., 10. 1952.
4. A.J. Youker, et al., Mo Recovery Updates and Physical Properties of Uranyl Sulfate Solutions, Argonne National Laboratory, ANL/CSE-13/20, Rev. 1, 2014.
5. Lloyd Conlin, et al., “Listing of Available ACE Data Tables”, LA-UR-13-21822, 2013
6. ANSYS-Fluent 17.2 Manual and Theory book.
7. L.D.P. King, “Design and Description of Water Boiler Reactor”, Proceedings of the International Conference on the Peaceful uses of Atomic Energy, 1955.
8. M.E. Bunker, “Status Report on the Water Boiler Reactor”, LA-2854, 1963.
9. Sergey Chemerisov, et al., “Experimental Results for Direct Electron Irradiation of a Uranyl Sulfate Solution: Bubble Formation and Thermal Hydraulics Studies”, ANL/NE-15/19.
10. Neil E. Todrease, Mujid S. Kazimi, “Nuclear System 1”, chapter 11.
11. Cynthia Buechler, “Aqueous Solution Vessel Thermal Model Development”, LA-UR-15-23537, 2015.
12. Cynthia Buechler, “Aqueous Solution Vessel Thermal Model Development II”, LA-UR-15-28444, 2015.

Appendix A: *Tritium Gas Target Neutron Production Rate*

Greg Dale
Accelerator Operations and Technology Division
Accelerators and Electrodynamics (AE)
Los Alamos National Laboratory
Los Alamos, NM 87544

Mass Stopping power: The Mass Stopping Power is defined as

$$S_m(E) = -\frac{1}{\rho}\frac{dE}{dx}$$

where, ρ is the density and dE/dx is the energy loss (dE) per differential path length (dx). The units of Mass Stopping power are generally MeV-cm^2/g. The Mass Stopping Power can be converted to the Stopping Power by multiplying by the target material's density. The stopping power is a function of energy, as shown in the figure below.

The figure below is a plot of the Mass Stopping Power data for a deuterium beam stopping in a tritium gas obtained with the SRIM Code.

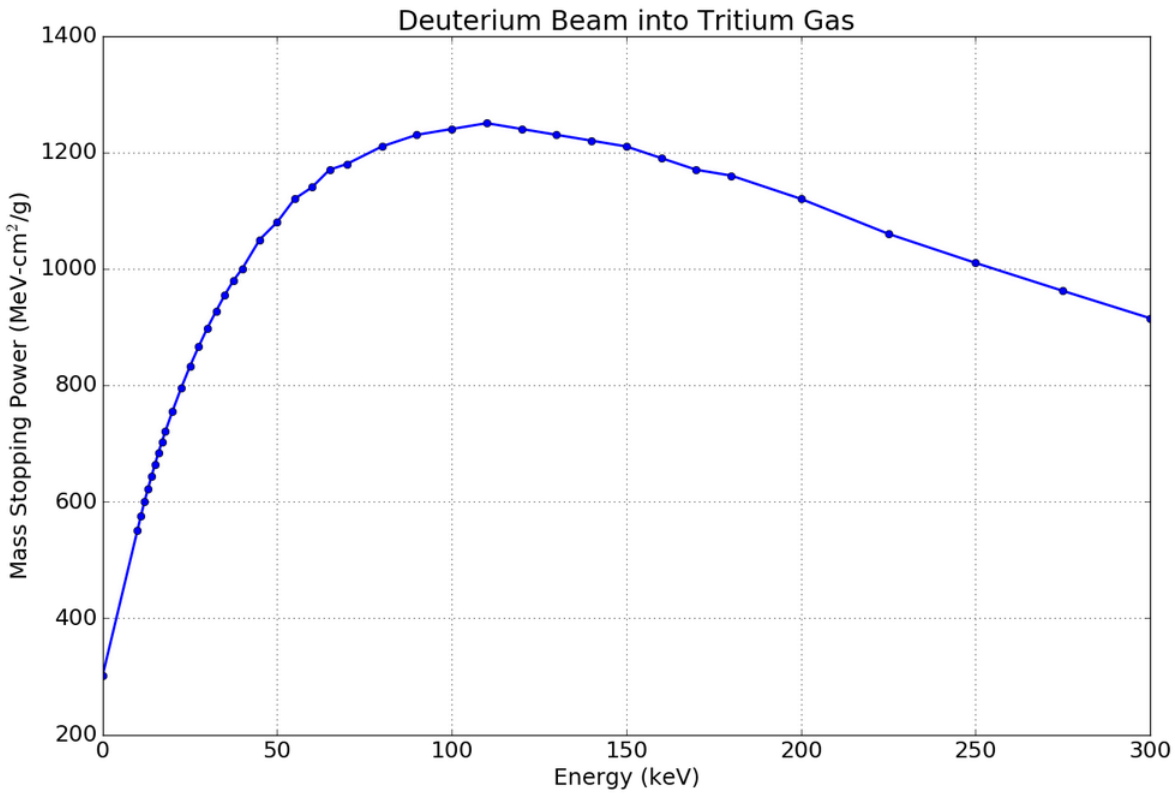

Gas Density: The density of an ideal gas as a function of temperature and pressure is given by

$$\rho(P,T) = \frac{MP}{RT}$$

where M is the atomic mass of the gas, P is the pressure, R is the gas constant, and T is the temperature. For pressure in Torr, temperature in Kelvin, and atomic mass in g/Mole, the gas constant is 62,360 cc-Torr/K/Mole. Calculate the tritium gas density for 8 Torr at 293 K. The atomic density is 5.2733 atoms/cc.

Stopping Power: The (regular) stopping power, Sp(E)=−dEdx is simply the mass stopping power multiplied by the target density. The stopping power for the density calculated above is plotted below. From here forward, it will be more convenient to use the stopping power in units of keV-cm2/g

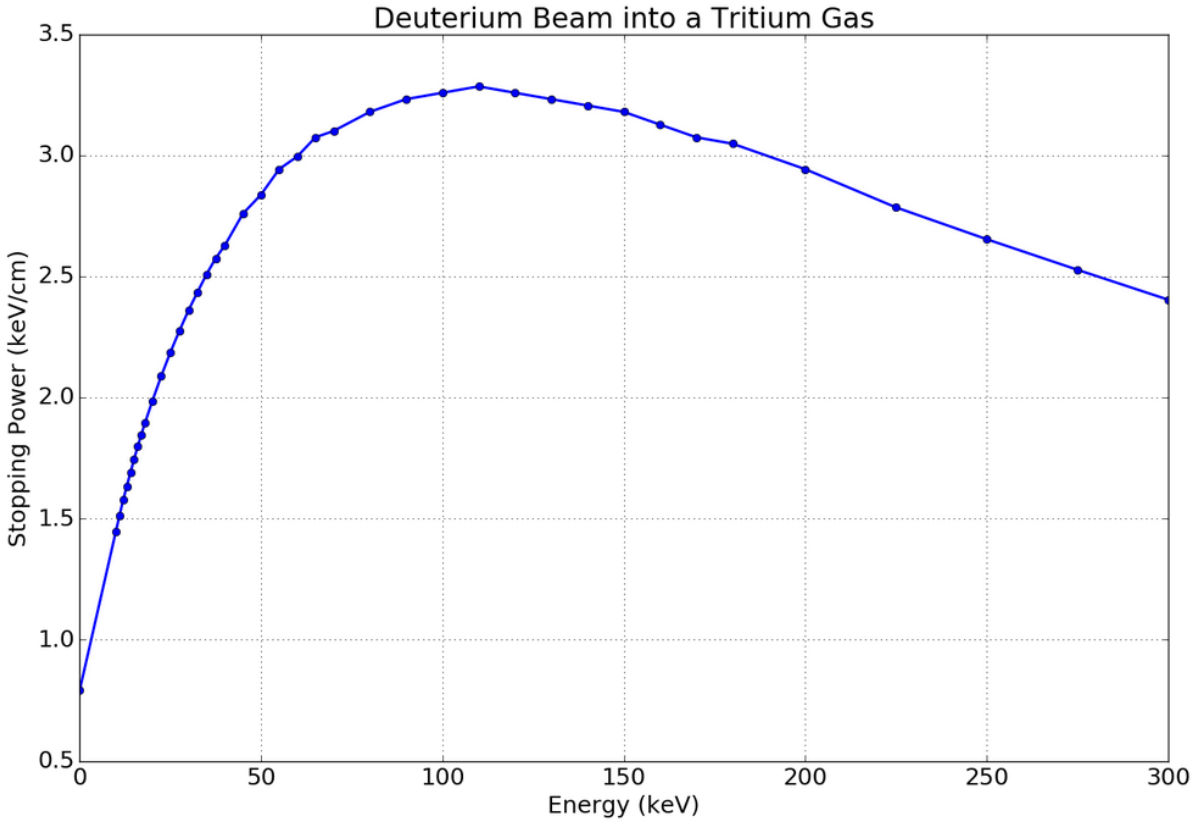

Beam Energy as a function of position: The ion range of a particle with an initial energy E in the continuous slowing down approximation (CSDA) can be calculated by integrating the reciprocal of the stopping power over energy

$$R(E) = \int_E^0 \frac{1}{\frac{dE}{dx}} dE = \int_0^E \frac{-1}{\frac{dE}{dx}} dE = \int_0^E \frac{1}{S_p(E)} dE$$

The range calculation provides numerical data for beam energy as a function of position. This is shown plotted below.

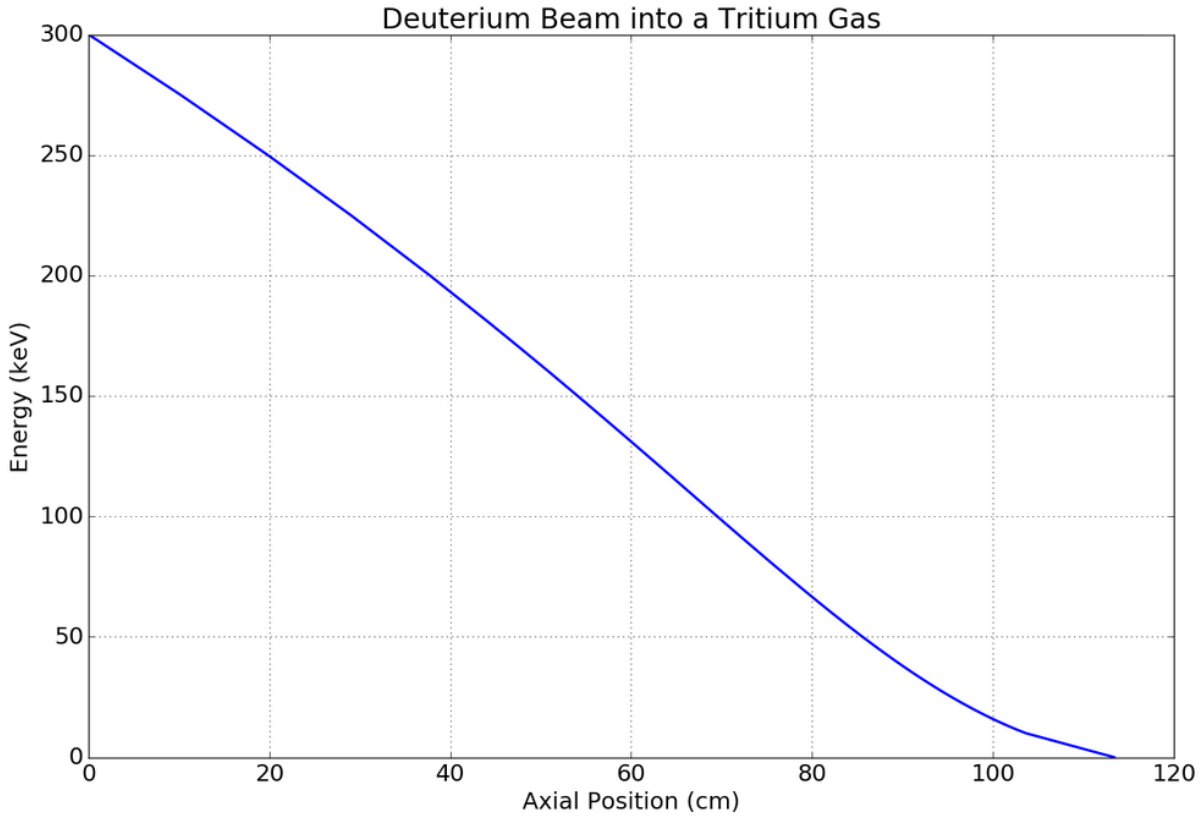

Neutron Production Rate (Neutron Yield per unit Length): The probability of a deuterium ion fusing with a stationary tritium atom is quantified via the thermonuclear fusion cross section, $\sigma_T(E)$. A fit for this cross section is given in the NRL Plasma Formulary as:

$$\sigma_T(E) = \frac{A_5 + [(A_4 - A_3E)^2 + 1]^{-1}A_2}{E[exp(A_1E^{1/2}) - 1}$$

where, A_1 = 45.95, A_2 = 50,200, A_3 = 1.368E-2, A_4 = 1.076, A_5 = 409

The D-T fusion cross section is plotted below in the energy range of interest.

The neutron yield density, which is the fusion neutron production rate per unit volume, is given by:

$$y(E) = \Phi N \sigma_T(E)$$

where N is the atomic density of the target gas and Φ is the incident deuterium ion flux. Assuming that the beam shape does not change as the deuterium ions slow down, the incident deuterium ion flux is equal to the ion beam current, I_b, divided by the charge of a deuterium ion, C_D and the cross sectional area of the beam, A.

$$\Phi = \frac{I_b}{C_D A}$$

Assuming a atomic deuterium beam, the charge of a deuterium ion is equal to 1.6E-19 C/deuterium. The units of deuterium ion flux are ions/cm^2/sec. combining the two equations above results in

$$y(E) = \frac{I_b}{C_D A} N \sigma_T(E)$$

Since $\sigma_T(E)$ is the only quantity which is a function of energy, and the ion energy can be described as a function of position, then the neutron yield density can be written as a function of axial position, z as

$$y(z) = \frac{I_b}{C_D A} N \sigma_T(E(z))$$

The total neutron production rate, Y is the integral of the neutron production rate overall volume.

$$Y = \int_V y(z) dV$$

Neutrons are only produced inside the beam area, so the integral perpendicular to the beam can be limited to the extent of the beam area as

$$Y = \int_0^L \int_A y(z) dA dz$$

where L is the total length of the tritium gas target. Substituting in for $y(z)$

$$Y = \frac{I_b N}{C_D A} \int_0^L \int_0^A \sigma_T(E(z)) dA dz$$

The integral over area is simply the cross sectional area of the beam, A, and this cancels with the A in the denominator resulting in

$$Y = \frac{I_b N}{C_D} \int_0^L \sigma_T(E(z)) dz$$

The neutron yield per unit length is a good intermediate result to plot from the data. This is given by

$$Y'(z) = \frac{dY}{dz}$$

$$= \frac{d}{dz}\frac{I_b N}{C_D}\int_0^L \sigma_T(E(z))dz$$

$$= \frac{I_b N}{C_D}\sigma_T(E(z))$$

The neutron yield per unit length normalized per unit beam current is given by

$$\frac{Y'(z)}{I_b} = \frac{N\sigma_T(E(z))}{C_D}$$

This is shown plotted in the figure below. Also shown is the beam energy as a function of position.

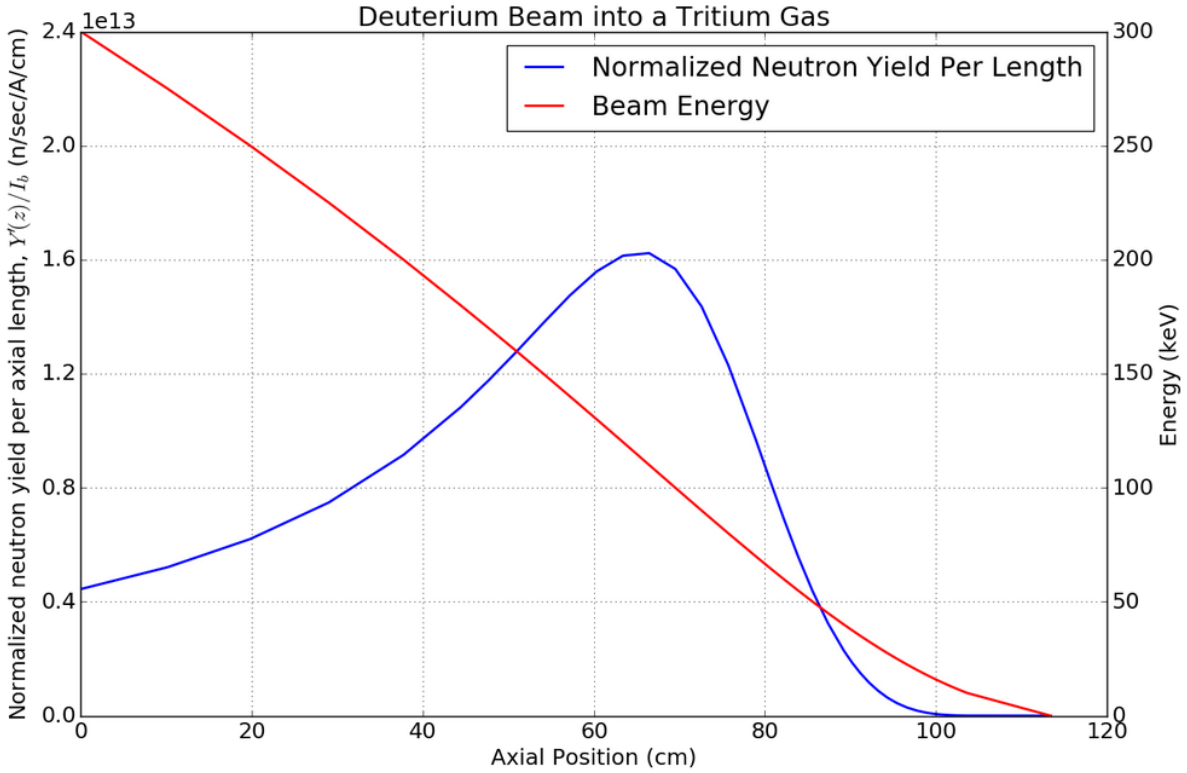

Appendix B: *Development of Uranyl Sulfate thermal property correlations using Multi-variable regression*

Thermal property correlations (i.e. Density, Viscosity, Thermal conductivity, and Specific heat) are developed based on measured data using multivariable regression method. The selected measurements for the correlation development are in the range of 20 to 90°C (temperature), and 90g-U/L-200g-U/L (Concentration). The developed thermal property correlations are used in the MCFD and MCNP simulations. The reference documents for the current study are listed below

1. Mo Recovery Updates and Physical Properties of Uranyl Sulfate Solutions, Argonne National Laboratory, ANL/CSE-13/20, Rev. 1, 2014.
2. The Densities of Uranyl Sulfate Solutions between 20° and 90°C, Mound Laboratory, MLM-728.

Density: Using multivariable regression method, a polynomial correlation as a function of concentration and temperature for the density of Uranyl Sulfate solution is calculated as shown in below equation.

$$Density\ \left(\frac{g}{mL}\right) = 7.16e-8X^2 + 0.0013\,X - 3.43e-6\,Y^2 - 0.00019Y + 1.0068$$

where, X = concentration (g-U/L), Y, temperature (C). Detailed M-regression calculation for density is listed in the calculation note below. A visualization of calculated correlation and experimental data is illustrated below. For example, the density of Uranyl Sulfate is calculated to be 1.168 g/mL when the concentration and temperature are set to 130gU/L, 50C, respectively.

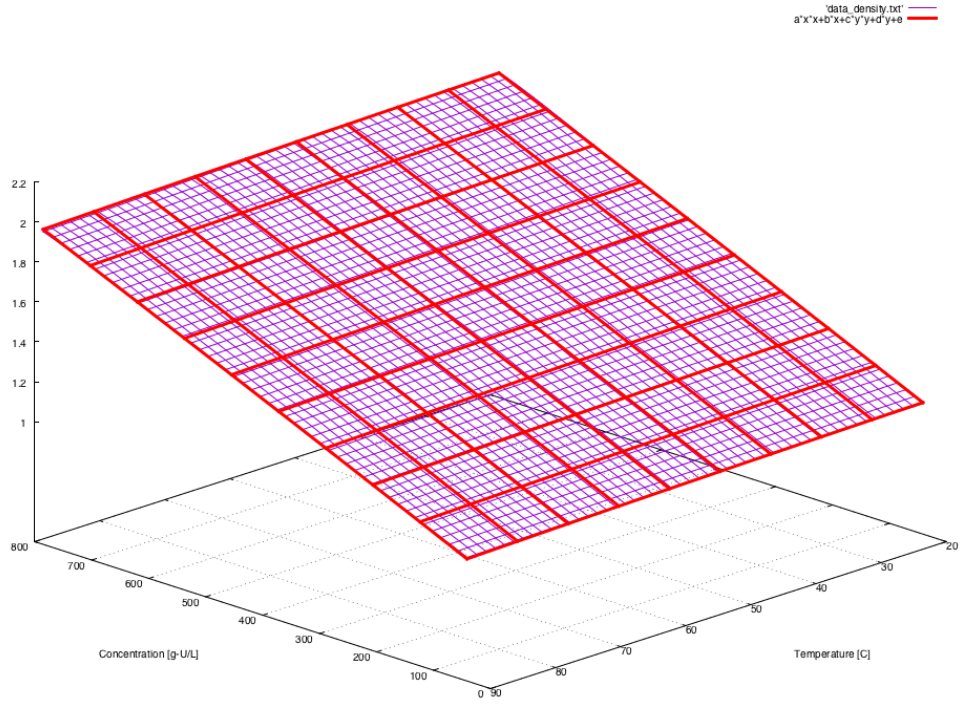

Viscosity: The viscosity correlation is listed below using the same M-regression method, and a visual comparison between data map and correlation is illustrated.

$$Viscosity(cp) = -6.61e-6\,X^2 + 0.0038\,X + 0.00023\,Y^2 - 0.038\,Y + 1.65$$

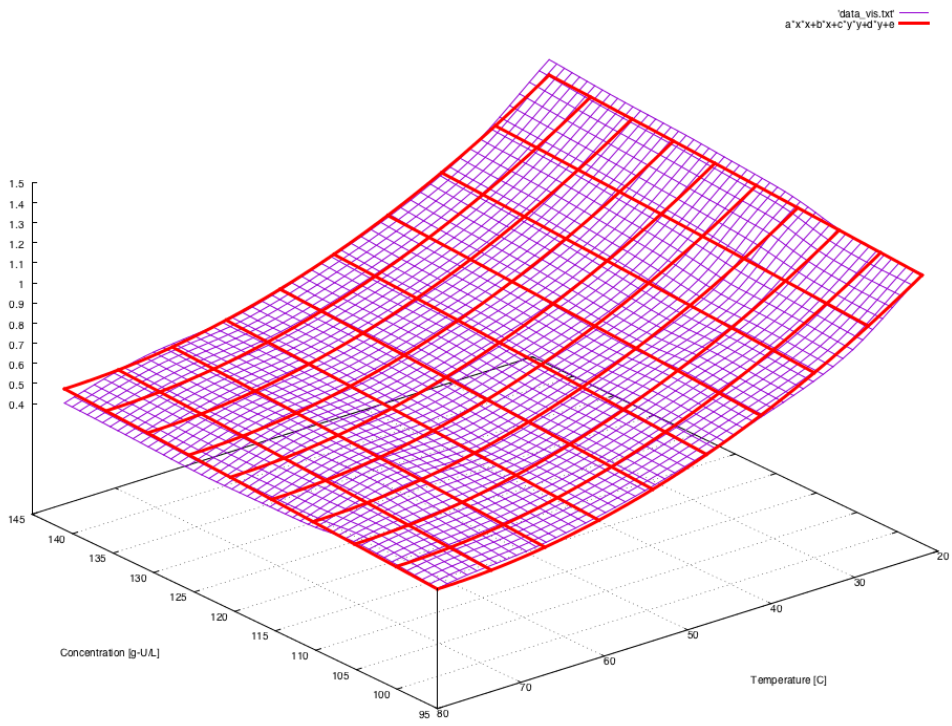

Thermal conductivity: The thermal conductivity correlation is listed below, and a visual comparison between measurement data and correlation is illustrated as follows.

$$Thermal\ conductivity\left(\frac{mW}{mK}\right) = 0.0069X^2 - 1.9X - 0.0015Y^2 + 1.19\,Y + 678.65$$

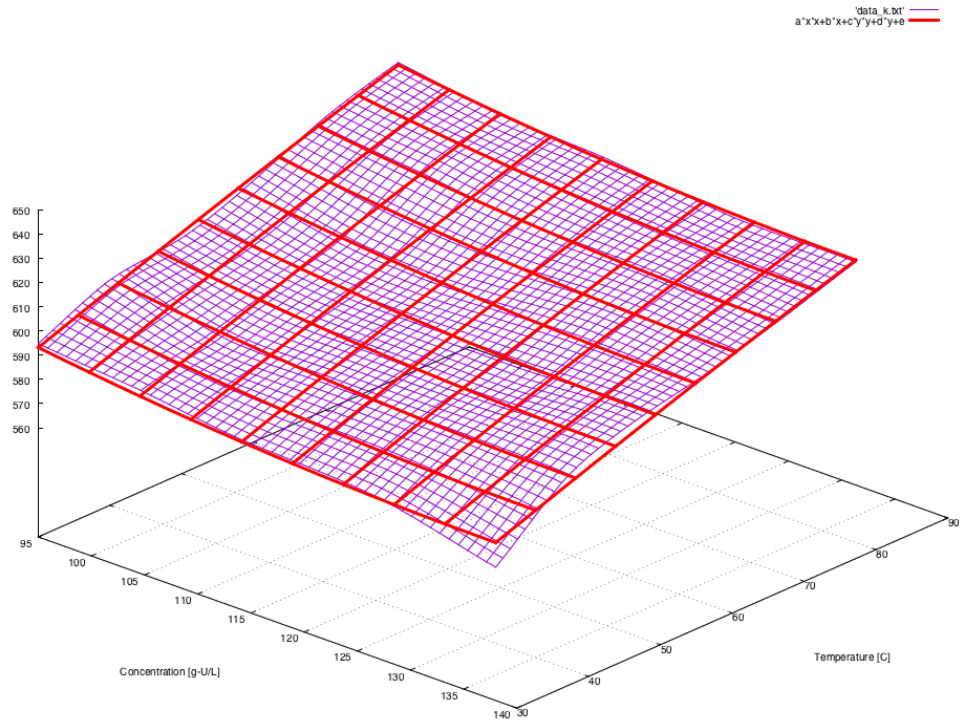

Specific heat: $Specific\ heat\ \left(\frac{J}{gK}\right) = 1.64e-5X^2 - 0.0094X + 3.23e-6Y^2 - 0.00063Y + 4.34$

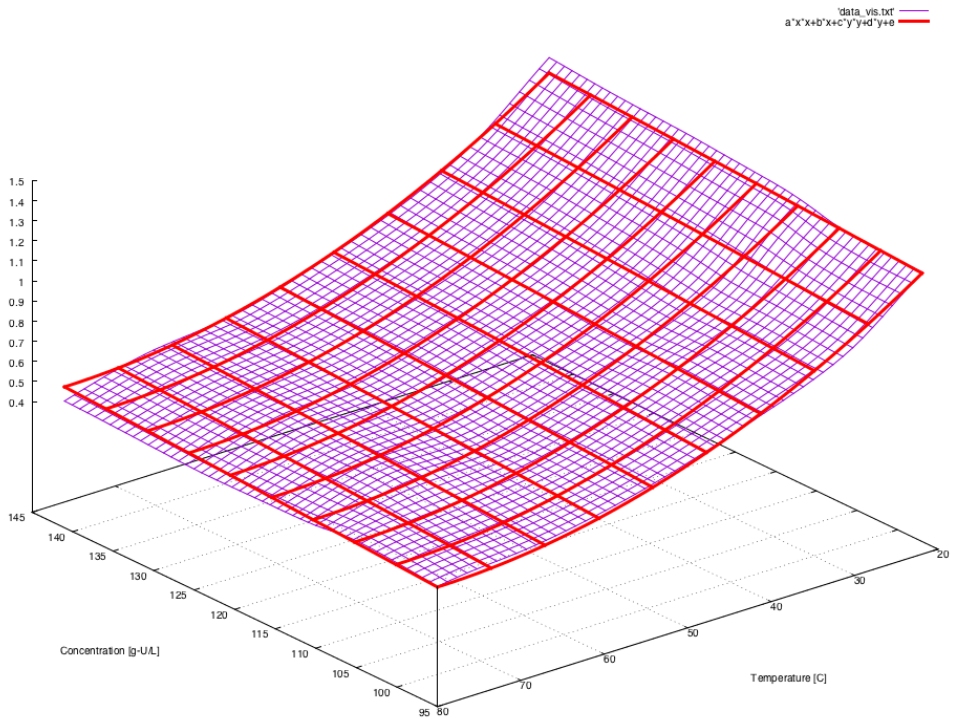

As a few examples of regression programing, multivariable-regression calculation note for density and viscosity are documented below in detail.

Density

****

```
gnuplot> f(x,y) = a*x*x +b*x + c*y*y +d*y +e
gnuplot> FIT_LIMIT = 1e-6
gnuplot> fit f(x,y) 'data_density.txt' using 1:2:3:(1) via a,b,c,d,e
        warning:
            > Implied independent variable t not found in fit function.
            > Assuming version 4 syntax with zerror in column 4 but no zerror keyword.

iter      chisq       delta/lim  lambda   a             b             c             d             e
  0 3.4783305716e+12   0.00e+00  1.03e+05   1.000000e+00   1.000000e+00   1.000000e+00   1.000000e+00   1.000000e+00
  1 8.3756309717e+08  -4.15e+09  1.03e+04  -6.046881e-03   9.966351e-01   9.120589e-01   9.988861e-01   9.999854e-01
  2 9.8081540355e+06  -8.44e+07  1.03e+03  -2.191802e-03   9.715166e-01   6.715928e-02   9.878502e-01   9.998310e-01
  3 2.9073750596e+05  -3.27e+07  1.03e+02  -7.986221e-04   5.591170e-01  -2.350469e-02   9.400883e-01   9.978399e-01
  4 1.7459624413e+03  -1.66e+08  1.03e+01   5.407278e-05  -5.377101e-02  -6.390847e-03   6.226960e-01   9.869632e-01
  5 9.8418098570e-01  -1.77e+09  1.03e+00   1.553177e-06  -1.957016e-04  -1.634295e-04   1.606447e-02   9.682942e-01
  6 1.1865905938e-03  -8.28e+08  1.03e-01  -5.846046e-08   1.349049e-03  -7.689834e-06   2.096380e-04   9.944320e-01
  7 6.9594069286e-04  -7.05e+05  1.03e-02  -3.833180e-08   1.329138e-03  -3.011585e-06  -3.432582e-04   1.011598e+00
  8 6.9592028544e-04  -2.93e+01  1.03e-03  -3.819850e-08   1.329006e-03  -2.981457e-06  -3.468229e-04   1.011709e+00
  9 6.9592028544e-04  -1.16e-07  1.03e-04  -3.819849e-08   1.329006e-03  -2.981455e-06  -3.468231e-04   1.011709e+00
iter      chisq       delta/lim  lambda   a             b             c             d             e

After 9 iterations the fit converged.
final sum of squares of residuals : 0.00069592
rel. change during last iteration : -1.16378e-13

degrees of freedom    (FIT_NDF)                       : 59
rms of residuals      (FIT_STDFIT) = sqrt(WSSR/ndf)    : 0.00343442
variance of residuals (reduced chisquare) = WSSR/ndf   : 1.17953e-05
p-value of the Chisq distribution (FIT_P)              : 1

Final set of parameters            Asymptotic Standard Error
=======================            ==========================
```

```
a               = -3.81985e-08     +/- 8.942e-09    (23.41%)
b               = 0.00132901       +/- 7.57e-06     (0.5696%)
c               = -2.98146e-06     +/- 9.014e-07    (30.23%)
d               = -0.000346823     +/- 0.0001003    (28.91%)
e               = 1.01171          +/- 0.002679     (0.2648%)

correlation matrix of the fit parameters:
                a      b      c      d      e
a               1.000
b              -0.963  1.000
c              -0.022  0.019  1.000
d               0.022 -0.015 -0.984  1.000
e               0.359 -0.419  0.803 -0.854  1.000
```

Viscosity

****

```
gnuplot> fit f(x,y) 'data_vis.txt' using 1:2:3:(1) via a,b,c,d,e
        warning:
                > Implied independent variable t not found in fit function.
                > Assuming version 4 syntax with zerror in column 4 but no zerror keyword.

iter      chisq       delta/lim  lambda   a             b             c             d             e
  0 1.0299941248e+10  0.00e+00  6.48e+03   1.000000e+00  1.000000e+00  1.000000e+00  1.000000e+00  1.000000e+00
  1 4.7678261398e+06  -2.16e+09  6.48e+02  -3.612892e-02  9.895526e-01  1.541183e-01  9.895462e-01  9.998957e-01
  2 1.3965831829e+04  -3.40e+08  6.48e+01  -8.795658e-03  9.651613e-01 -1.260123e-02  9.776963e-01  9.994771e-01
  3 1.5430922328e+03  -8.05e+06  6.48e+00  -2.279148e-03  1.891332e-01 -7.275687e-03  6.273799e-01  9.862059e-01
  4 1.5605137182e+00  -9.88e+08  6.48e-01   5.096290e-05 -1.059868e-02 -4.344499e-04  3.191785e-02  9.825752e-01
  5 4.2052117742e-02  -3.61e+07  6.48e-02  -5.288628e-05  1.493088e-02  2.319834e-04 -3.744577e-02  9.966771e-01
  6 3.8646646484e-02  -8.81e+04  6.48e-03  -2.172642e-05  7.484371e-03  2.359467e-04 -3.786523e-02  1.442836e+00
  7 3.8244245892e-02  -1.05e+04  6.48e-04  -6.690932e-06  3.891959e-03  2.373616e-04 -3.801541e-02  1.656850e+00
  8 3.8244236633e-02  -2.42e-01  6.48e-05  -6.618466e-06  3.874644e-03  2.373684e-04 -3.801614e-02  1.657882e+00
iter      chisq       delta/lim  lambda   a             b             c             d             e

After 8 iterations the fit converged.
final sum of squares of residuals : 0.0382442
rel. change during last iteration : -2.42108e-07

degrees of freedom    (FIT_NDF)                        : 30
rms of residuals      (FIT_STDFIT) = sqrt(WSSR/ndf)    : 0.0357045
variance of residuals (reduced chisquare) = WSSR/ndf   : 0.00127481
p-value of the Chisq distribution (FIT_P)              : 1

Final set of parameters            Asymptotic Standard Error
=======================            ==========================
a               = -6.61847e-06     +/- 2.728e-05    (412.2%)
b               = 0.00387464       +/- 0.006485     (167.4%)
c               = 0.000237368      +/- 1.971e-05    (8.304%)
d               = -0.0380161       +/- 0.002037     (5.357%)
e               = 1.65788          +/- 0.3828       (23.09%)

correlation matrix of the fit parameters:
                a      b      c      d      e
a               1.000
b              -0.998  1.000
c               0.011 -0.013  1.000
d              -0.010  0.011 -0.988  1.000
```

Appendix C: *MCNP input for the solution vessel power calculation*

```
Lattice Trial with lots of contents
11 1 -1.1854 -8 -220 68 80 82 84 86
      700 702 704 706 800 802 804 806 imp:n=1 $ core
111 0 -8 220 68 80 82 84 86
      700 702 704 706 800 802 804 806 imp:n=1 $ above fuel up to 222
122 0 -8 222 -65 imp:n=1  $ above center after 222
13 33 -6.56 -10 8 imp:n=1 $ RV
50 0  12 imp:n=0 $ world
52 4 -0.998 13 -12 imp:n=1  $ water pool
53 4 -0.998 10 -11 imp:n=1 $ outer_water_5mm
55 29 -2.70 11 -13 imp:n=1 $ aluminum cask_thickness_5mm
56 0 -58 -222 imp:n=1 $ central thimble
65 13 -19.25 58 -65 -222 imp:n=1  $ moderator=tunsgen
67 4 -0.9830 65 -67 -20 imp:n=1  $ cooling jacket
68 33 -6.56 67 -68 -20 imp:n=1   $ inner fuel wall
C Tube cell
70 4 -0.983 -701 -20 imp:n=1 $ CR 1
71 33 -6.56 701 -700 -20 imp:n=1 $ CR 1 wall
72 4 -0.983 -703 -20 imp:n=1 $ CR 2
73 33 -6.56 703 -702 -20 imp:n=1 $ CR 2 wall
74 4 -0.983 -705 -20 imp:n=1 $ CR 3
75 33 -6.56 705 -704 -20 imp:n=1 $ CR 3 wall
76 4 -0.983 -707 -20 imp:n=1 $ CR 4
77 33 -6.56 707 -706 -20 imp:n=1 $ CR 4 wall
80 4 -0.983 -801 -20 imp:n=1 $ CR 5
81 33 -6.56 801 -800 -20 imp:n=1 $ CR 5 wall
82 4 -0.983 -803 -20 imp:n=1 $ CR 6
83 33 -6.56 803 -802 -20 imp:N=1 $ CR 6 wall
84 4 -0.983 -805 -20 imp:n=1 $ CR 7
85 33 -6.56 805 -804 -20 imp:n=1 $ CR 7 wall
86 4 -0.983 -807 -20 imp:n=1 $ CR 8
87 33 -6.56 807 -806 -20 imp:N=1 $ CR 8 wall
800 4 -0.983 -81 -20 imp:n=1  $ CR 9
801 33 -6.56 81 -80 -20 imp:n=1 $ CR 9 wall
802 4 -0.983 -83 -20 imp:n=1  $ CR 10
803 33 -6.56 83 -82 -20 imp:n=1 $ CR 10 wall
804 4 -0.983 -85 -20 imp:n=1  $ CR 11
805 33 -6.56 85 -84 -20 imp:N=1 $ CR 11 wall
806 4 -0.983 -87 -20 imp:n=1  $ CR 12
807 33 -6.56 87 -86 -20 imp:n=1 $ CR 12 wall

8 rcc 0 0 -30 0 0 150 35  $ core
10 rcc 0 0 -30.5 0 0 151 35.500 $ RV
11 rcc 0 0 -31 0 0 152 36 $ outer water gap_5mm
13 rcc 0 0 -31.5 0 0 153 36.5 $ outer aluminium 5mm thickness
12 rcc 0 0 -60 0 0 200.0 60.0  $ pool
58 rcc 0 0 -30 0 0 150 8.5    $ gas bottle  cooling jacket
65 rcc 0 0 -30 0 0 150 16.5    $  moderator
```

```
67 rcc 0 0 -30 0 0 150 17.0    $ cooling jacket
68 rcc 0 0 -30 0 0 150 17.5 $ inner fuel wall
C   tubes surfaces
700 rcc 26.25 0 -30 0 0 150 1.0
701 rcc 26.25 0 -30 0 0 150 0.8
702 rcc -26.25 0 -30 0 0 150 1.0
703 rcc -26.25 0 -30 0 0 150 0.8
704 rcc 0 26.25 -30 0 0 150 1.0
705 rcc 0 26.25 -30 0 0 150 0.8
706 rcc 0 -26.25 -30 0 0 150 1.0
707 rcc 0 -26.25 -30 0 0 150 0.8
80 rcc 22.73 -13.13 -30 0 0 150 1.0
81 rcc 22.73 -13.13 -30 0 0 150 0.8
800 rcc 22.73 13.13 -30 0 0 150 1.0
801 rcc 22.73 13.13 -30 0 0 150 0.8
82 rcc 13.13 -22.73 -30 0 0 150 1.0
83 rcc 13.13 -22.73 -30 0 0 150 0.8
802 rcc 13.13 22.73 -30 0 0 150 1.0
803 rcc 13.13 22.73 -30 0 0 150 0.8
84 rcc -22.73 -13.13 -30 0 0 150 1.0
85 rcc -22.73 -13.13 -30 0 0 150 0.8
804 rcc -22.73 13.13 -30 0 0 150 1.0
805 rcc -22.73 13.13 -30 0 0 150 0.8
86 rcc -13.13 -22.73 -30 0 0 150 1.0
87 rcc -13.13 -22.73 -30 0 0 150 0.8
806 rcc -13.13 22.73 -30 0 0 150 1.0
807 rcc -13.13 22.73 -30 0 0 150 0.8
220 pz 75.3   $ fuel level
222 pz 100.0  $ core height
20 pz 150.0   $ coolant height

mode N P
SDEF POS=0 0 70 ERG=14 AXS=0 0 -1 EXT=d1 RAD=d2 PAR=1
si1 A   0
       5.31 10.60 15.90 21.20 26.50 31.80 37.10
       42.50 47.80 53.10 58.40 63.70 69.00 74.30
       79.60 84.90 90.20 95.50 100
sp1     5.00e+12 5.51e+12 6.07e+12 6.76e+12
       7.61e+12 8.60e+12 9.88e+12 1.14e+13 1.33e+13 1.54e+13 1.73e+13
       1.83e+13 1.66e+13 1.21e+13 6.56e+12 2.42e+12 4.88e+11 2.76e+10
       2.99e+9 0
si2     0  0.5642    $ Source extends to 1cm^2 area
sp2     -21  1       $ Sample weighted as r^1 to correct for geometric effects
TOTNU
C    2.369e+05 0.95
vol  2.848e+05 0 0 0 0 0 0 0 0 0 0 0 0 0 0 0 0 0 0 0 0 0 0 0 0 0 0 0
    0 0 0 0 0 0 0 0 0
C Uranyl Sulfate Solution
m1    92235.80c 7.2476E-05 92238.80c 2.9077E-04
     1001.80c 6.6356E-02
```

```
      8016.80c 3.5358E-02
      16032.80c 3.6325E-4
      16033.80c 2.5683e-06
      16034.80c 1.4554E-5
      16036.80c 3.4244e-08
mt1   lwtr.10t
C Light water
m4    1001.80c 2 8016.80c 1
mt4   lwtr.10t
C Tungsten(W)
m13   74180.80c 0.12
      74182.80c 26.50
      74183.80c 14.31
      74184.80c 30.64
      74186.80c 28.43
C Aluminum
m29   13027.80c 1
C Zircaloy4 Zr:0.996, Fe:0.002, Cr:0.001, O:0.001 Tn(1.5%) composition is not included here
m33   40090.80c -5.0503e-1
      40091.80c -1.1136e-1
      40092.80c -1.7209e-1
      40094.80c -1.7820e-1
      40096.80c -2.9320e-2
      8016.80c -0.001
      26054.80c -1.1291e-4
      26056.80c -1.8380e-3
      26057.80c -4.3206e-5
      26058.80c -5.8507e-6
      24050.80c -5.6145e-5
      24052.80c -9.1656e-4
      24053.80c -2.1575e-5
      24054.80c -2.9254e-6
C carbon steel
C m43 1002.50c 2 8016.50c 1
C mt43    hwtr.20t
C m36   92235.50c 20 92238.50c 80
C    Be
C m27  4009.50c 1
C
C mt27 be.01t
C    B4C
C m39  5010.50c 90 5011.50c 10 6000.50c 25
C    graphite
C
C m28  6000.80c 1
C mt28 grph.20t
THTME 0
TMP1  2.96e-08 2.52e-08 2.52e-08 2.52e-08 2.52e-08 2.52e-08 2.52e-08 2.52e-08
      2.52e-08 2.52e-08 2.52e-08 2.52e-08 2.52e-08 2.52e-08
      2.52e-08 2.52e-08 2.52e-08 2.52e-08 2.52e-08 2.52e-08 2.52e-08 2.52e-08
```

```
     2.52e-08 2.52e-08 2.52e-08 2.52e-08 2.52e-08 2.52e-08 2.52e-08 2.52e-08
     2.52e-08 2.52e-08 2.52e-08 2.52e-08 2.52e-08 2.52e-08
C kcode 5000 1 50 250
C ksrc 20 0 20 -20 0 20 0 20 20 0 -20 20
C      -20 0 25 -37 0 25
C       0 20 25 0 37 25
C       0 -20 25 0 -37 25
FMESH14:N  GEOM=cyl ORIGIN=0 0 -30
         IMESH=8.8175 16.8175 18.135 33.8 IINTS=1 6 1 16
         JMESH=97.4209 JINTS=50
         KMESH=1 KINTS=1
         AXS=0 0 1 VEC=1 0 0 OUT=ij
fm14  (-1 1 -6)
f4:N 11
fc4  hpfb fissions in solution
C     2.344e+05 0.95
fm4  -2.369e+05 1 -6
e4   1.0e-07 1.0e-06 1.0e-05 1.0e-04 1.0e-03 1.0e-02 0.1 1 15 T
C f14:n 65
C fc14  fissions in moderator
C fm14  -1.963e+04 12 -6
C e14  1.0e-07 1.0e-06 1.0e-05 1.0e-04 1.0e-03 1.0e-02 0.1 1 15 T
NPS  1e5
TMESH
cmesh3
cora3  0 16.5 25i 36
corb3 -33 54i 77
corc3 2 28 360
C corc3 2 28 32 58 62 88 92 118 122 148 152 178 182 208 212 238 242 268 272 298 302 328
332 358 360
cmesh1:n
cora1  0 16.5 25i 36 60
corb1 -31 50i 71
corc1 360
cmesh11:n
cora11  0 16.5 25i 36 40
corb11 -31 50i 71
corc11 360
ENDMD
fm11  (-1 1 -6)
```